Gyro-kinetic theory and global simulations of the collisionless tearing instability: The impact of trapped particles through the magnetic field curvature

D. Zarzoso (iD), S. Nasr, X. Garbet (iD), A. I. Smolyakov (iD), and S. Benkadda (iD)

View Online   Export Citation   CrossMark

Gyro-kinetic theory and global simulations of the collisionless tearing instability: The impact of trapped particles through the magnetic field curvature

View Online   Export Citation   CrossMark

D. Zarzoso,[1] (iD) S. Nasr,[1] X. Garbet,[2] (iD) A. I. Smolyakov,[3] (iD) and S. Benkadda[1] (iD)

AFFILIATIONS

[1]Aix-Marseille Université, CNRS PIIM, UMR 7345 Marseille, France
[2]CEA, IRFM, F-13108 St. Paul-lez-Durance Cedex, France
[3]Department of Physics and Engineering Physics, University of Saskatchewan, Saskatoon, Saskatchewan S7N 5E2, Canada

ABSTRACT

The linear instability of the tearing mode is analyzed using a gyrokinetic approach within a Hamiltonian formalism, where the interaction between particles and the tearing mode through the wave-particle resonance is retained. On the one hand, the curvature of the magnetic field is shown to play no role in the linear instability when only passing particles are present in the plasma. On the other hand, the presence of trapped particles leads to an overall increase in the growth rate. Gyrokinetic simulations using the state-of-the-art GKW code confirm these findings and are further used to investigate the impact of the magnetic field curvature and the temperature gradient on tearing modes including the effect of trapped particles. Without the temperature gradient, wave-particle resonance with the trapped electrons tends to stabilize the tearing mode, while with the finite temperature gradient, the magnetic curvature tends to destabilize the tearing mode, suggesting an interchange mechanism. The balance of these two stabilizing/destabilizing effects leads to a threshold in the temperature gradient beyond which the magnetic curvature plays a destabilizing role. This opens the way for a deeper understanding and control of the tearing instability in fusion plasmas.

Published by AIP Publishing. https://doi.org/10.1063/1.5109947

I. INTRODUCTION

In magnetized laboratory and space plasmas, a special class of instabilities, called tearing instability, can occur in the presence of non-ideal effects (such as resistivity or inertia) and can tear apart the magnetic field lines, resulting in their reconnection. This process leads to a modification of the magnetic topology, characterized by the formation of magnetic islands. In space conditions, they are considered to be important for dynamics and energy release in the magnetotail.[1] In laboratory magnetically confined plasmas, tearing modes enhance particle and energy transport, degrading this way the overall confinement. In particular, they have been proved to result in fast ion losses[2,3] and even lead to catastrophic disruptions.[4] Therefore, the understanding of the tearing mode is of prime importance in space and laboratory plasmas.

The tearing mode instability has been extensively studied in the framework of magnetohydrodynamics (MHD) theory.[5,6] For many situations in space conditions and high temperature tokamak plasmas, regimes can be considered as weakly collisional and kinetic considerations are therefore required.[1,7,8] In the tearing mode theory, usually

the outer (ideal) and inner (inertial and resistive) regions can be separated. The stability of large scale islands in the MHD regime is determined by the global current profile effects, which introduce the so-called Δ' parameter determined from the outer region and which has to be positive for the instability. The modifications of Δ' by magnetic profiling and kinetic effects due to trapped particles were considered in Ref. 9. The other mechanisms, related to the temperature gradients and collisions, are important locally (in the inner inertial-resistive layer). They have been studied in various settings[7,10–12] and were recognized as important destabilizing mechanisms for $\Delta' < 0$. In collisionless regimes, the electron inertia replaces the resistivity to support the instability.[7,13,14]

Future tokamaks are expected, however, to operate at very low collisionality, and various collisionless effects need to be considered together with magnetic field geometry. Toroidal effects due to the magnetic field curvature have been studied in fluid theory.[6,15] However, gyrokinetic theory provides the most comprehensive framework for studies of kinetic effects in low collisional regimes and

complex magnetic geometries and has been widely used for tearing mode studies.[16–23]

Within the framework of gyrokinetic theory, the trajectories of the guiding-centers in tokamaks can be analyzed. They have complex structures, characterized by different frequencies and scales. In general, particles can be classified into two groups: (1) trapped particles, whose trajectories are localized on the low field side of the torus in the magnetic mirrors formed by toroidicity, and (2) passing particles, which can circulate fully along the magnetic field lines and complete a poloidal turn. The special role of trapped particles in tearing mode stability has been recognized in analytical[24] and numerical studies.[25,26] It was found that trapped particle resonances contribute to the destabilization of microtearing modes in low collisionality regimes.[25–29] In this paper, we investigate resonant effects of passing and trapped particles on tearing modes in collisionless regimes. This is done using analytical theory and global gyrokinetic simulations, through which we also perform an extensive parametric study of the tearing instability with emphasis on the effects of the magnetic field curvature and particle resonances.

The remainder of this paper is structured as follows: in Sec. II, we derive, within the gyrokinetic approach, the perturbed parallel current using a Hamiltonian formalism. Section III is devoted to the derivation of the tearing mode dispersion relation. This is done by integration of Ampère's law, under the so-called constant-ψ approximation, and separating the radial domain into an ideal MHD (outer) region where kinetic effects are negligible and where we calculate numerically the Δ' stability parameter and a nonideal (inner) region where kinetic effects are retained through the wave-particle resonance. In Sec. IV, the different resonances between the tearing mode and the particles are studied analytically and the presence of trapped particles is shown to increase the growth rate of the instability. We also show that the magnetic curvature does not play any role in the tearing instability when only passing particles are considered. Section V is devoted to the numerical analysis using GKW simulations. In particular, we confirm the analytical results and study in detail the impact of trapped particles, curvature, and temperature gradient. In Sec. VI, we report on the different responses of particles to the tearing instability through energy exchange diagnostics and evidence of the interaction between trapped particles and the tearing mode is provided.

II. HAMILTONIAN FORMALISM TO CALCULATE THE PERTURBED PARALLEL CURRENT WITHIN A GYROKINETIC APPROACH

The tearing instability can be described at the simplest level using Ampère's law,

$$\nabla \times (\nabla \times \mathbf{A}) = \mu_0 \mathbf{j}, \tag{1}$$

where $\mathbf{A}$ is the vector potential, $\mathbf{j}$ is the current, and μ_0 is the vacuum permeability. We assume that we have only the parallel component of $\mathbf{A}$. Therefore, $\mathbf{A} = A_\parallel \mathbf{b}$, where $\mathbf{b}$ is the unit vector along the magnetic field lines. Projecting onto the parallel direction straightforwardly gives an equation for the perturbed parallel current $j_\parallel$,

$$\nabla_\perp^2 A_\parallel = -\mu_0 j_\parallel, \tag{2}$$

which has to be integrated to obtain the dispersion relation. In Eq. (2), $\nabla_\perp^2$ is the Laplacian operator in the direction perpendicular to the equilibrium magnetic field.

In the following, we assume that the main response is that of electrons. Therefore, in order to calculate the perturbed parallel current, we will first of all calculate the exact linear response of electrons, which will yield the perturbed parallel current after integration in velocity space. The details of this calculation are given in Appendix A, where we follow closely the formalism used in Ref. 30. The idea is to start with the Vlasov equation in conservative form using a Hamiltonian formalism,

$$\frac{\partial F}{\partial t} - [\mathcal{H}, F] = 0, \tag{3}$$

where $[X, Y]$ represents the Poisson brackets between X and Y, i.e., $[X, Y] = \partial_\mathbf{x} X \partial_\mathbf{p} Y - \partial_\mathbf{p} X \partial_\mathbf{x} Y$, where $\mathbf{x}$ and $\mathbf{p}$ are the position and momenta, forming a set of canonical variables satisfying Hamilton's equations. We can introduce another system of canonically conjugated variables, satisfying Hamilton's equations, especially suitable for the analysis of particles in a tokamak, since they reflect the three directions of periodicity of the trajectories. These are the angle-action variables $\boldsymbol{\alpha}, \mathbf{J}$, with $\boldsymbol{\alpha} = (\alpha_1, \alpha_2, \alpha_3)$ and $\mathbf{J} = (J_1, J_2, J_3)$, where α_1 represents the gyrophase, α_2 represents the periodicity angle in the poloidal direction, and α_3 represents the periodicity angle in the toroidal direction. The actions are motion invariants associated with each direction of the particle trajectory. In particular, $J_1 = m_e \mu / (e Z_e)$, where e is the elementary charge, Z_e is the charge number (in the special case of electrons, $Z_e = -1$), and $\mu = m_e v_\perp / (2B)$ is the magnetic moment, with $v_\perp$ being the projection of the electron velocity onto the direction perpendicular to the magnetic field and B the modulus of the magnetic field. The second action, J_2, is written in terms of the toroidal flux of the magnetic field Φ as $J_2 = e Z_e \Phi + \frac{1}{2\pi} \oint m_e v_\parallel \, d\ell$, where ℓ is the coordinate along the magnetic field line and $v_\parallel$ is the component of the guiding-center velocity parallel to the magnetic field. Finally, the third action J_3 is the toroidal canonical momentum, $J_3 \equiv P_\varphi = -e Z_e \psi + m_e R v_\varphi$, with ψ being the poloidal flux of the magnetic field, R being the major radius, and v_φ being the projection of the electron velocity onto the toroidal direction.

We anticipate that we will calculate the parallel current for highly passing electrons, for which J_2 is closer to a function of the radial coordinate than J_3, i.e., we can make the approximation $J_2 \approx e Z_e \Phi(r)$, which will introduce the gradients of the equilibrium with respect to the radial coordinate. This is why we change variables $\mathbf{J} \to \mathbf{I} = (J_1, J_2, \mathcal{H}_{eq})$, where $\mathcal{H}_{eq}$ is the equilibrium Hamiltonian, representing the energy in the absence of any perturbation. Following Hamilton's equations, the time derivative of the angles is $\dot{\boldsymbol{\alpha}} = \partial_\mathbf{J} \mathcal{H} \equiv \boldsymbol{\Omega}$, where we have introduced the three frequencies of motion, satisfying the ordering $\Omega_1 \gg \omega, \Omega_2, \Omega_3$, with ω being the frequency of the tearing mode. The distribution function and the Hamiltonian are decomposed into equilibrium and perturbed parts. By definition, the equilibrium quantities do not depend on the angles, but only on the actions. This allows us to linearize the Vlasov equation and, owing to the periodicity of the perturbations with respect to the angles $\boldsymbol{\alpha}$, we can write the perturbed distribution function and Hamiltonian as Fourier series $\{\delta F, \delta \mathcal{H}\} = \sum_{\omega, \mathbf{n}} \{\delta F_{\mathbf{n}, \omega}, \delta \mathcal{H}_{\mathbf{n}, \omega}\} \exp(i(\mathbf{n} \cdot \boldsymbol{\alpha} - \omega t))$. After some algebra, it can be shown that the exact linear solution of the Vlasov equation is written as

$$\delta F_{\mathbf{n}, \omega} = \frac{\partial F_{eq}}{\partial \mathcal{H}_{eq}} \delta \mathcal{H}_{\mathbf{n}, \omega} + \frac{1}{B} \frac{\partial F_{eq}}{\partial \mu} \delta \mathcal{H}_{\mathbf{n}', \omega}$$
$$- \frac{\omega \partial_{\mathcal{H}_{eq}} F_{eq} + n_2 \partial_{J_2} F_{eq}}{\omega - \mathbf{n}^\star \cdot \boldsymbol{\Omega}} \delta \mathcal{H}_{\mathbf{n}^\star, \omega}, \tag{4}$$

where $\mathbf{n}' = (n_1 \neq 0, n_2, n_3)$ and $\mathbf{n}^\star = (n_1 = 0, n_2, n_3)$.

The perturbed parallel current is calculated as

$$j_\parallel = eZ_e \int \mathrm{d}^3\mathbf{p}\left(v_{\parallel,eq}\delta F + \delta v_\parallel F_{eq}\right), \qquad (5)$$

where the perturbed parallel velocity is expressed in terms of the parallel vector potential,

$$\delta v_\parallel = -\frac{eZ_e}{m_e}A_\parallel. \qquad (6)$$

The perturbed parallel velocity proportional to the vector potential plays an essential role in canceling the adiabatic response of electrons in the calculation of the perturbed parallel current, as can be observed in (B10). This is the so-called *cancelation problem*, often invoked within the framework of PIC simulations.[31] In order to continue further with analytical calculations, we assume an equilibrium distribution function,

$$F_{eq} = \frac{n_{eq}}{\left(2\pi T_{eq}/m_e\right)^{3/2}}\mathrm{e}^{-\frac{\mathcal{H}_{eq}-\mathcal{U}_{eq}}{T_{eq}}}, \qquad (7)$$

which satisfies $\partial_{\mathcal{H}_{eq}}F_{eq} = -F_{eq}/T_{eq}$. In the previous expression, $\mathcal{U}_{eq}$ is a function which depends on the motion invariants and represents the departure from the zero-mean-velocity Maxwellian equilibrium. In this paper, in order to generate an equilibrium parallel current, $\mathcal{U}_{eq}$ is an odd function of $v_\parallel$. The perturbed parallel current will be written in normalized units. For this purpose, we normalize the velocities to the thermal velocity of electrons v_{th}, the distances to R_0, the frequencies to the transit frequency $\omega_t = v_{th}/R_0$, the equilibrium distribution function to n_0/v_{th}^3, with n_0 being some normalizing density, the parallel vector potential to $B_0 R_0 \rho_\star^2$, and the temperature to a normalizing temperature defined as $T_0 = m_e v_{th}^2/2$. Using the perturbed distribution function given by Eq. (4) and considering only deeply passing electrons, we show in Appendix B that the perturbed parallel current can be expressed as

$$j_\parallel(\mathbf{x},t) = \rho_\star en_0 v_{th}\frac{2}{\hat{T}_{eq}}\sum_{m,n,\omega}\left\langle\hat{v}_\parallel^2\frac{\hat{\omega}-\hat{\omega}_{\star g}}{\hat{\omega}-\hat{k}_\parallel\hat{v}_\parallel-\hat{\omega}_D}\right\rangle$$
$$\times \hat{A}_{\parallel m,n,\omega}(\mathbf{x})\mathrm{e}^{i(m\theta+n\varphi-\omega t)}, \qquad (8)$$

where m and n are the poloidal and toroidal mode numbers, respectively. Note that, in general, the previous expression implies an infinite sum over all the wave-numbers and frequencies, but in the following, we will simply project onto one single mode. The angles have been replaced by θ and φ, representing the poloidal and toroidal angles, respectively. The symbol $\hat{\cdot}$ indicates the normalized quantities, the parallel wave vector $k_\parallel$ is given by $k_\parallel = (m/q + n)/R_0$, and the magnetic drift frequency ω_D is given by $\omega_D = 2qn/r(m_e v_{\parallel,eq}^2 + \mu B_0)/(eZ_e B_0 R_0)$, with q being the safety factor characterizing the helicity of the magnetic field lines and R_0 and B_0 the major radius and the modulus of the magnetic field, respectively, evaluated both at the magnetic axis. The notation $\langle\cdots\rangle$ has been introduced to represent an average over gyrocenter equilibrium velocity space weighted by the equilibrium distribution function,

$$\langle\cdots\rangle = \int \mathcal{J}\mathrm{d}v_{\parallel,eq}\mathrm{d}\mu\,\cdots\,F_{eq}, \qquad (9)$$

with $\mathcal{J}$ being the jacobian of the transformation. Notice that $k_\parallel$ vanishes on the rational surface defined as $q = -m/n$. In the remainder of

this paper, the eq subscript for the parallel velocity will be dropped for the sake of simplicity. Note that $\rho_\star$ gives the typical ordering between the equilibrium and the perturbed distribution function and $en_0 v_{th}$ is the normalization for the current. In this expression, we have introduced the generalized diamagnetic frequency $\omega_{\star g} = mT_{eq}\partial_{J_2}\log F_{eq}$, which includes the spatial dependence of the equilibrium. For thermal passing particles, at lowest order in $\rho_\star$, one can write $J_2 \approx eZ_e\Phi$. Therefore, the derivative with respect to J_2 can be reduced to a derivative with respect to the radial position.

III. GYROKINETIC DISPERSION RELATION OF THE TEARING INSTABILITY

In order to derive the dispersion relation of the tearing instability, we make use of Ampère's law, given by Eq. (2), where we introduce expression (8) for the perturbed parallel current. Ampère's law can also be written using normalized quantities and projecting onto one single (m, n, ω) Fourier mode,

$$\hat{\delta}_e^2\hat{\nabla}_\perp^2\hat{A}_{\parallel m,n,\omega}(\mathbf{x}) = \frac{2}{\hat{T}_{eq}}\left\langle\hat{v}_\parallel^2\frac{\hat{\omega}-\hat{\omega}_{\star g}}{\hat{\omega}-\hat{k}_\parallel\hat{v}_\parallel-\hat{\omega}_D}\right\rangle\hat{A}_{\parallel m,n,\omega}(\mathbf{x}), \qquad (10)$$

where $\hat{\delta}_e = \delta_e/R_0$ and $\delta_e = \sqrt{m_e/\mu_0 e^2 n_0}$ is the electron skin depth. The dispersion relation of the tearing mode is obtained integrating equation (10), but for this purpose, we need to give convenient equilibrium quantities that will allow us to perform analytical calculations.

Regarding the equilibrium distribution function F_{eq}, we assume that it is given by expression (7), where the $\mathcal{U}_{eq}$ term represents a shift in the parallel velocity, which leads to an equilibrium parallel current. In normalized units, it takes the form

$$\hat{F}_{eq} = \frac{\hat{n}_{eq}}{(\pi\hat{T}_{eq})^{3/2}}\exp\left(-\frac{\hat{v}_\parallel^2+\hat{v}_\perp^2-2\hat{v}_\parallel\hat{u}_e}{\hat{T}_{eq}}\right), \qquad (11)$$

where we assume that $\hat{u}_e$ depends only on P_φ and verifies the ordering $u_e^2 \ll v_\parallel^2$ (small shift in $v_\parallel$). In addition, we assume circular concentric magnetic surfaces. The magnetic field is therefore given by the simplified expression $\mathbf{B} = B_0 R_0(r/q(r)R_0\mathbf{e}_\theta + \mathbf{e}_\varphi)/R$, with $\mathbf{e}_\theta$ and $\mathbf{e}_\varphi$ being unit vectors in the poloidal and toroidal directions, respectively, and $q(r)$ the safety factor as a function of the minor radius r. The poloidal flux is then written as

$$\psi(r) = B_0\int_0^r\frac{r'}{q(r')}\mathrm{d}r', \qquad (12)$$

and the toroidal flux satisfies the equation

$$\frac{\mathrm{d}\Phi}{\mathrm{d}\psi} = -q(r). \qquad (13)$$

Therefore, the expression for the generalized diamagnetic frequency can be written as follows:

$$\omega_{\star g} = \frac{mT_{eq}}{e}\frac{1}{rB_0}\left[\frac{1}{n_{eq}}\frac{\mathrm{d}n_{eq}}{\mathrm{d}r}\right.$$
$$\left.+\frac{1}{T_{eq}}\frac{\mathrm{d}T_{eq}}{\mathrm{d}r}\left(\frac{v_\parallel^2}{v_{th}^2}+\frac{\mu B}{T_{eq}}-\frac{2v_\parallel u_e}{v_{th}^2}-\frac{3}{2}\right)+2\frac{v_\parallel}{v_{th}^2}\frac{\mathrm{d}u_e}{\mathrm{d}r}\right]. \qquad (14)$$

Note that we keep the electron mean parallel velocity, together with its radial gradient. However, in the following, the assumption is made that $u_e \ll v_{\rm th}$, so that the term multiplying the temperature gradient simplifies to the standard $E/T_{\rm eq} - 3/2$. Nevertheless, the radial derivative $\mathrm{d}u_e/\mathrm{d}r$ is kept. Therefore, the diamagnetic frequency can be split into standard density and temperature terms, $\omega_{\star n}$ and $\omega_{\star T}$, respectively, and the term $\omega_{\star u}$ coming from the radial gradient of the parallel velocity, i.e.,

$$\omega_{\star g} = \omega_{\star n} + \omega_{\star T} + \omega_{\star u} \equiv \omega_\star + \omega_{\star u}, \qquad (15)$$

where the notation $\omega_\star$ has been used to gather both density and temperature gradients. Using normalized quantities, each of these frequencies read

$$\hat{\omega}_\star = \rho_\star \hat{T}_{\rm eq} \frac{m}{2\hat{r}} \left[\frac{1}{\hat{n}_{\rm eq}} \frac{\mathrm{d}\hat{n}_{\rm eq}}{\mathrm{d}\hat{r}} + \frac{1}{\hat{T}_{\rm eq}} \frac{\mathrm{d}\hat{T}_{\rm eq}}{\mathrm{d}\hat{r}} \left(\hat{E} - \frac{3}{2} \right) \right], \qquad (16)$$

$$\hat{\omega}_{\star u} = \rho_\star \frac{m}{\hat{r}} \hat{v}_\parallel \frac{\mathrm{d}\hat{u}_e}{\mathrm{d}\hat{r}}. \qquad (17)$$

The mean parallel velocity must be related to the safety factor by Ampère's law applied to the equilibrium. In the cylindrical limit, Ampère's law in normalized units can be approximated as

$$\frac{\rho_e R_0}{\delta_e^2} \hat{J}_{\rm eq} = \frac{1}{\hat{r}} \frac{\mathrm{d}}{\mathrm{d}\hat{r}} \left(\frac{\hat{r}^2}{q} \right), \qquad (18)$$

where the equilibrium current is obtained from the integration of the equilibrium distribution function,

$$J_{\rm eq} = eZ_e \int \mathcal{J} \mathrm{d}v_\parallel \mathrm{d}\mu v_\parallel F_{\rm eq}, \qquad (19)$$

with $\mathcal{J} = 2\pi B/m_e$. The equilibrium parallel current is then $J_{\rm eq} = eZ_e n_{\rm eq} u_e$, and in normalized units,

$$\hat{J}_{\rm eq} = Z_e \hat{n}_{\rm eq} \hat{u}_e. \qquad (20)$$

Unless stated otherwise, in the following, the $\hat{}$ symbol will be dropped for the sake of simplicity and all quantities are assumed to be normalized. We assume that the gradient of the equilibrium parallel current is mainly due to the gradient of the mean electron parallel velocity. Therefore, one can integrate the normalized Ampère's law to obtain the expression of the safety factor in terms of the integrated mean velocity,

$$q(r) = \frac{\delta_e^2}{\rho_e R_0 Z_e n_{\rm eq}} \frac{r^2}{\int_0^r \mathrm{d}r' r' u_e(r')}. \qquad (21)$$

Therefore, differential equation (10) can be written using only the radial profile of the safety factor, which yields the linear dispersion relation of the tearing mode. Nevertheless, solving analytically this dispersion relation in the whole radial domain for general profiles of density, temperature, and electron velocity is rather arduous. Therefore, the tearing mode dispersion relation is solved by splitting it into two linear differential equations that will be solved in two different regions of the radial domain: an ideal outer region and a narrow resonant layer. For each region, we will make some assumptions. In the resonant layer, $|k_\parallel| \ll 1$, and therefore, the whole resonance $\omega - k_\parallel v_\parallel$

must be kept leading to the ordering $\omega \approx k_\parallel v_{\rm th}$; however, in the ideal region, $|\omega| \ll |k_\parallel v_\parallel|, |\omega_{\star g}|$. The two solutions are matched by considering the so-called constant-ψ approximation[5] that assumes that the perturbed parallel scalar potential of the magnetic field is constant inside the nonideal layer.

A. The tearing mode equation in the outer (ideal MHD) region

In the ideal region where $\omega_{\star g} \gg \omega$ and $k_\parallel v_\parallel \gg \omega, \omega_D$ the expression in between brackets of Eq. (10) reads

$$\left\langle v_\parallel^2 \frac{\omega - \omega_{\star g}}{\omega - k_\parallel v_\parallel - \omega_D} \right\rangle = \left\langle v_\parallel^2 \frac{\omega_\star}{k_\parallel v_\parallel} \right\rangle. \qquad (22)$$

Since $\omega_\star$ ($\omega_{\star u}$, respectively) is an even (odd, respectively) function in $v_\parallel$, the only remaining term in the numerator of expression (22) is $\omega_{\star u}$. This leads to the differential equation

$$\delta_e^2 \nabla_\perp^2 A_{\parallel m,n,\omega}(\mathbf{x}) = -\rho_\star n_{\rm eq} \frac{m}{r k_\parallel} \frac{\mathrm{d}u_e}{\mathrm{d}r} A_{\parallel m,n,\omega}(\mathbf{x}). \qquad (23)$$

Using the relation between the safety factor and the mean electron parallel velocity given by Eq. (21) and assuming again that the density gradient does not affect significantly the parallel current gradient, we can write

$$\frac{\mathrm{d}^2 A_\parallel(r)}{\mathrm{d}r^2} + \frac{1}{r} \frac{\mathrm{d}A_\parallel(r)}{\mathrm{d}r} - \frac{m^2}{r^2} A_\parallel(r) = \Lambda(r) A_\parallel(r), \qquad (24)$$

where we have noted $A_\parallel \equiv \delta A_{\parallel m,n,\omega}$ for simplicity and

$$\Lambda(r) = \frac{-3s + 2s^2 - r^2 q''(r)/q(r)}{r^2 \left(1 + q(r)\dfrac{n}{m} \right)}, \qquad (25)$$

where s is the magnetic shear defined as $s = rq'(r)/q(r)$, with q' and q'' representing the first and second derivatives of the safety factor with respect to r, respectively. We consider that $q > 1$, $q' > 0$, and $q'' > 0$ for all r. We will also suppose that there is a radial position r_s such that $q(r_s) = -m/n$. This means that $r < r_s \Rightarrow q(r) < -m/n$ and $r > r_s \Rightarrow q(r) > -m/n$. Then, for $r < r_s$ ($r > r_s$, respectively), we have the inequality $\Lambda(r) < 0$ (resp. > 0), which means that for $A_\parallel > 0$, the second derivative must be negative (positive, respectively), and therefore, the solution is concave (convex, respectively). In addition, note that $\lim_{r \to r_s^\pm} \Lambda(r) = \pm\infty$. This means that the first derivative is discontinuous at the position $r = r_s$, which allows us to define the parameter Δ',[5]

$$\Delta' = \lim_{\varepsilon \to 0} \frac{A_\parallel'(r_s + \varepsilon) - A_\parallel'(r_s - \varepsilon)}{A_\parallel(r_s)}, \qquad (26)$$

where $A_\parallel'$ denotes the derivative of $A_\parallel$ with respect to r. This parameter represents the jump of the solution across the resonant surface, and it will be used as a matching parameter between the solution in the inner region and the solution in the outer region. In normalized units, we have $\hat{\Delta}' = R_0 \Delta'$. In the following, only the normalized values of the Δ' parameter are used.

Equation (24) can be solved using the shooting method[32] for a general q profile, but in the following, we use a q profile of the Wesson-type,[33]

$$q(r) = q_a \frac{r^2/\epsilon^2}{1 - (1 - r^2/\epsilon^2)^{\nu+1}}, \qquad (27)$$

where q_a is the value of the safety factor at the position $r = a$ and ν is a parameter that controls the current density peaking. The solution of the tearing mode equation in the outer region is presented in Fig. 1 for three different values of the parameter ν and fixing $q_a = 3.5$ and the aspect ratio $R_0/a = 0.3$. The boundary conditions $A_\parallel(r_{\min}) = A_\parallel(r_{\max}) = 0$ are used, and at the resonant surface $r = r_s$, we fix a normalized value $A_\parallel(r_s) = 1$.

In Fig. 2, we show the contours of Δ' in solid black lines scanning over q_a and ν. The dotted magenta lines denote the position of the resonant surface. The dashed blue line presents the limit $q(r_{\min}) = 1$. The domain of interest for the analysis of the $(m, n) = (2, -1)$ mode relies above that limit. Beneath it, the mode would coexist with the $(m, n) = (1, -1)$ mode. In the same figure, the asterisks represent the simulations that will be analyzed in Sec. V, which are localized in the region $q(r_{\min}) > 1$, exploring increasing values of Δ'. In Sec. III B, we assume that the value of Δ' is known and determined from the outer solution, and we use it to solve the tearing equation in the inner layer.

B. The tearing mode equation in the inner region

In the region around the resonant surface, $k_\parallel \ll 1$, and therefore, the resonance in the expression in between brackets of Eq. (10) is kept as it is. Due to parity reasons, the contribution from $\omega_{\star u}$ in the numerator can be neglected, so that the tearing mode equation reads

$$\delta_e^2 \nabla_\perp^2 A_{\parallel m,n,\omega}(\mathbf{x}) = \frac{2}{T_{eq}} \left\langle v_\parallel^2 \frac{\omega - \omega_\star}{\omega - k_\parallel v_\parallel - \omega_D} \right\rangle A_{\parallel m,n,\omega}(\mathbf{x}). \qquad (28)$$

We assume that the width of the resonant layer is 2Δ. Integrating the equation over this region yields

$$\delta_e^2 \int_{-\Delta}^{\Delta} \frac{d^2 A_\parallel}{dx^2} dx = A_\parallel(0) \int_{-\Delta}^{\Delta} \Lambda dx, \qquad (29)$$

where we have again noted $A_\parallel \equiv A_{\parallel m,n,\omega}$ and the so-called constant-ψ approximation has been made, assuming that the solution is constant in the resonant layer. In addition, to perform the integration in the
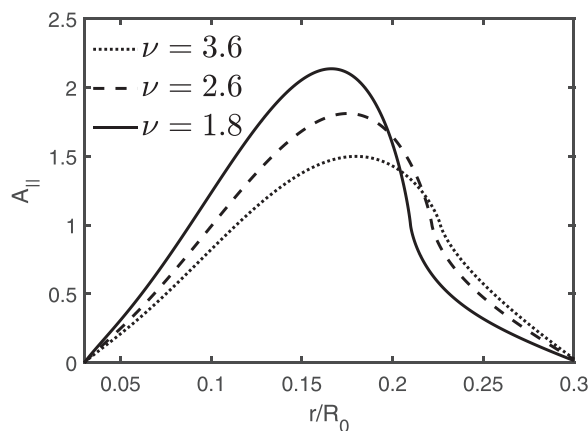
FIG. 1. The tearing mode eigenfunction for different values of ν, $q_a = 3.5$, and $\epsilon = 1/3.3$.
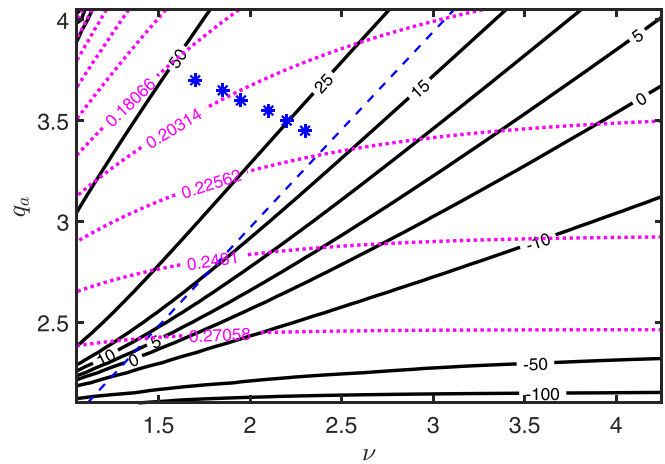
FIG. 2. Contours of Δ' (solid black) and the resonant surface position r_s (dotted magenta) as a function of the q profile parameters ν and q_a. The blue dashed line denotes the limit $q(r_{\min}) = 1$, and the blue asterisks denote where in this diagram the simulations shown in Sec. V lie. Δ' is normalized to R_0^{-1}, and r_s is normalized to R_0.

resonant layer, the assumption of slab geometry is made, such that $\nabla_\perp^2 \equiv d^2/dx^2$, where $x = (r - r_s)/R_0$ represents the distance to the rational surface at the radial position r_s, normalized to R_0. This assumption is justified due to the small width of the resonant layer and is applied in this paper only to simplify the analytical calculations. Moreover, the coefficient Λ is now given by the more general expression,

$$\Lambda = \frac{2}{T_{eq}} \left\langle v_\parallel^2 \frac{\omega - \omega_\star}{\omega - k_\parallel v_\parallel - \omega_D} \right\rangle. \qquad (30)$$

The integral on the left hand-side of Eq. (29) gives $\Delta' A_\parallel(0)$. For the integral on the right-hand side, we change variable $v_\parallel' = -v_\parallel$ and $x' = -x$ to the negative domain of the space integral. In addition, since the perturbed parallel current is localized in a very narrow region around the resonant surface, we can extent the integral with respect to the radial distance to infinity without introducing significant errors. Under these assumptions, the collisionless tearing mode dispersion relation in the magnetic limit is expressed in normalized units as

$$\delta_e^2 \Delta' = \frac{8 n_{eq}}{T_{eq}^{5/2} \sqrt{\pi}} \int_0^{+\infty} dx \int_{-\infty}^{+\infty} dv_\parallel \int_0^{+\infty} v_\perp dv_\perp v_\parallel^2 e^{-\frac{v_\parallel^2 + v_\perp^2}{T_{eq}}}$$
$$\times \frac{\omega - \omega_\star}{\omega - k_\parallel(x) v_\parallel - \omega_D}. \qquad (31)$$

In this expression, the parallel wave vector can be expressed as $k_\parallel(x) = k_y/L_s x = k_\parallel' x$, with L_s being the magnetic shear scale length and $k_y = m/r$, and the diamagnetic frequency is expressed as

$$\omega_\star = \omega_{\star n} \left[1 + \eta_e \left(v^2 - \frac{3}{2} \right) \right], \qquad (32)$$

where $v^2 = v_\parallel^2 + v_\perp^2$, $\omega_{\star n} = \rho_\star T_{eq} m/2r n_{eq}'/n_{eq}$, and $\eta_e = (n_{eq}'/n_{eq})/(T_{eq}'/T_{eq})$.

IV. ANALYTICAL SOLUTION OF THE TEARING MODE DISPERSION RELATION

It is not straightforward to compute the integral (31). In order to shed some light on the underlying physics, we make first of all the assumption that all the particles are deeply passing. Afterward, we assume that only a fraction of the electron population is deeply passing and then analyze its effect on the tearing instability.

A. Solution of the dispersion relation with only passing particles

As a first step, we neglect the curvature and gradient of the magnetic field in the magnetic drift, such that $\omega_D = 0$ and only the $k_\parallel v_\parallel$ resonance is taken into account, i.e., the resonance with the parallel motion $\omega - k_\parallel v_\parallel$. In this case, since the denominator does not depend on the perpendicular velocity, we can first of all perform the integral with respect to $v_\perp$. Second, the velocity space integral can be performed using the plasma dispersion function and its derivatives as defined in Ref. 34.

After some algebra, the dispersion relation of the tearing mode reads

$$i\delta_e^2 \Delta' = \frac{4 n_{eq}\sqrt{\pi}}{\sqrt{T_{eq}}|k_\parallel'|}\left[\omega - \omega_{\star n}\left(1 + \left(2T_{eq} - \frac{3}{2}\right)\eta_e\right)\right]. \quad (33)$$

Writing $\omega = \omega_r + i\gamma$, where ω_r is the real frequency and γ is the growth rate, the solution of Eq. (33) reads[8]

$$\gamma = \frac{1}{4\sqrt{\pi}}\frac{\sqrt{T_{eq}}}{n_{eq}}\delta_e^2 |k_\parallel'|\Delta', \quad (34)$$

$$\omega_r = \omega_{\star n}\left[1 + \left(2T_{eq} - \frac{3}{2}\right)\eta_e\right]. \quad (35)$$

Strictly speaking, if one chooses the normalization constant T_0 as the value of the temperature at the resonant surface, in this case, $T_0 = T_{eq}$, i.e., $\hat{T}_{eq} = 1$. Then, the background density and temperature profiles do not change the growth rate of the mode; however, they additionally make the mode oscillate with a real frequency that scales linearly with the density and temperature gradients. It is important to note that we have taken into account density and temperature gradients in the local approximation. This means that although we consider radial profiles of the background quantities, they are evaluated locally. Therefore, they enter the equation as constant values on the resonant surface. Of course, a more rigorous approach is to consider the radial dependence of the profiles. However, this makes the x-integral too complicated to be solved analytically. The effect of profiles will be evaluated more adequately in Sec. V through gyrokinetic simulations using the GKW code.

We look now into the effects of the inhomogeneity of the magnetic field on the stability of the tearing mode. This means that the term containing the toroidal effects is kept in the resonant term of Eq. (31). Of course, the concept of toroidicity in slab geometry is quite contradictory. In fact, several assumptions are made for the magnetic drift ω_D. First, we consider the local approximation, meaning that the x-dependence is omitted, but the derivative with respect to x can be nonzero. Therefore, the geometry term $\mathbf{b} \times \nabla B$ responsible for the curvature of the magnetic field can be treated as a parameter in the equation. Second, all oscillations in the perpendicular direction are

neglected, and we assume them to be at the low field side of the tokamak where $\theta = 0$. Thus, the toroidal coupling between modes is not considered.

Integrating first over the radial direction allows us to make no assumption on the dependence of ω_D on the velocity space. Then, using the Gaussian integrals for the velocity space, we obtain the same expressions for the frequency and growth rate as those given in Eq. (34). A more accurate calculation can be performed by considering that the magnetic drift is actually a differential operator in the poloidal angle, which introduces nonlocal effects due to mode-mode coupling. It can be shown that even when these effects are taken into account, the mode frequency and growth rate are not modified. The details of the calculations are not given here for the sake of readability and clarity, but the interested reader can find the complete calculation in Appendix D.

Therefore, when considering only passing particles, and in the collisionless magnetic limit, the drift of particles due to the magnetic field inhomogeneity and curvature does not have an impact on the stability of the mode.

B. Correction due to the presence of trapped electrons

To consider the impact of trapped electrons on the stability of the tearing mode, we need to use the resonant response given by expression (4), which is the one valid for both passing and trapped electrons, since no assumption on their orbits was made at that step. For trapped particles, $\Omega_2 \gg \omega, \Omega_3$. Therefore, for a resonance to occur, the only possibility is $n_2 = 0$. This is mathematically equivalent to performing a bounce-average of the Vlasov equation. The resonance then reduces to $\omega - n_3\Omega_3$. In Appendix C, we show that for trapped particles, the precessional frequency is proportional to the magnetic drift [see Eq. (C30)]. In the absence of magnetic drift, the response of trapped particles to the tearing mode is purely nonresonant. Therefore, trapped particles do not contribute to the growth rate and the response of the whole electron population is reduced to the response of deeply passing electrons. Note that even if the response was resonant, it can be shown (see Appendix E) that the Hamiltonian of deeply trapped particles in the absence of magnetic drift vanishes. Thus, the velocity integral in Eq. (31) must be performed only in the passing domain $|v_\parallel| > \sqrt{2\varepsilon}|v_\perp|$ and the growth rate and frequency finally read

$$\gamma = \frac{1}{4\sqrt{\pi}}\frac{\sqrt{T_{eq}}}{n_{eq}}\delta_e^2 |k_\parallel'|\Delta' (1 + 2\varepsilon), \quad (36)$$

$$\omega = \omega_{\star n}\left[1 + \left(2T_{eq} - \frac{3}{2}\right)n_{eq}\right]. \quad (37)$$

Therefore, when a fraction of the electron population is magnetically trapped, the growth rate of the tearing mode is increased by a factor $1 + 2\epsilon$. Physically, this can be understood as follows.[24] The free energy for the tearing mode to be excited comes from the radial gradient of the equilibrium parallel current. This free energy is encapsulated in the stability parameter Δ'. Therefore, the free energy comes from the ideal region outside the resonant layer. This energy is subsequently transferred to particles within the resonant layer, where kinetic effects must be retained. The difference between the free energy that the mode takes from the ideal region and the energy that the mode transfers to the particles in the resonant layer is the energy available for the mode to grow. Since deeply trapped electrons do not contribute to this

transfer of energy, there is an increase in energy available for the mode to grow, resulting in an increased growth rate.

When the magnetic drift is taken into account, a resonance can occur between the tearing mode and the precessional motion of trapped particles, opening a new channel of energy transfer from the mode to the particles and therefore stabilizing the mode. The analytical calculation of the modification of the growth rate in the presence of trapped particles and magnetic drift is not straightforward. Therefore, we use a gyrokinetic code for the remaining analysis.

V. LINEAR GYROKINETIC SIMULATIONS OF COLLISIONLESS TEARING MODES WITH GKW

The self-consistent treatment of tearing modes requires radial profiles. For this reason, the global version of the gyrokinetic code GKW[35] is used. In this section, we provide a brief description of the code and then we present the implementations required for the excitation of the tearing mode in GKW.

A. The gyrokinetic model in GKW

The code GKW solves the gyrokinetic equations. The full details can be found in Ref. 35 and references therein. Here, we outline the basic set of linear equations that are solved. As in our theoretical approach presented in Sec. II, the δF approximation is used. The equation for the perturbed distribution function, for each species, is

$$\frac{\partial g_s}{\partial t} + \left(v_\parallel \mathbf{b} + \mathbf{v}_D\right) \cdot \nabla \delta F_s - \frac{\mu_s}{m_s}\frac{\mathbf{B} \cdot \nabla B}{B}\frac{\partial \delta F_s}{\partial v_\parallel} = S(F_{\mathrm{eq},s}), \quad (38)$$

where $g_s = \delta F_s + (Z_s e/T) v_\parallel \langle A_\parallel \rangle F_{\mathrm{eq},s}$, $\mu = m_s v_\perp^2/2B$ is the magnetic moment, $v_\parallel$ is the velocity along the magnetic field, and m_s and Z_s are the particle mass and charge number for species s, respectively. The drift velocity due to the gradient and curvature of the magnetic field is $\mathbf{v}_D = (1/Z_s e)(m_s v_\parallel^2 + \mu_s B)/B \mathbf{B} \times \nabla B/B^2$. Note that the nonlinear term $(\mathbf{v}_{E\times B} \cdot \nabla g_s$, where $\mathbf{v}_{E\times B}$ is the $\mathbf{E} \times \mathbf{B}$ velocity) is not taken into account in this linear study. $S(F_{\mathrm{eq},s})$ is the source term which is determined by the equilibrium distribution function of species s. The last term of the left-hand side of Eq. (38) is responsible for the trapping of particles (the so-called μ-grad$B$ or mirror term). The temperature and density profiles have the radial form,

$$n(r) = n_0 \exp\left[-\frac{R}{L_n}w\tanh\left(\frac{r-r_0}{w}\right)\right], \quad (39)$$

$$T(r) = T_0 \exp\left[-\frac{R}{L_T}w\tanh\left(\frac{r-r_0}{w}\right)\right], \quad (40)$$

where the distances are normalized to R_0, w is the width of the region where the gradient is localized, R/L_n, R/L_T, n_0, and T_0 are the logarithmic density gradient, logarithmic temperature gradient, density, and temperature, respectively, all evaluated at the reference radius r_0. All the normalizations in the code are consistent with the ones used so far in the present paper. The electrostatic potential is calculated from the gyrokinetic quasineutrality equation given by

$$\sum_s Z_s e \int (J_0 \cdot \delta F_s)^\dagger \mathcal{J}_s \mathrm{d}v_\parallel \mathrm{d}\mu_s$$
$$+ \sum_s \frac{Z_s^2 e^2}{T_s} \int \left(\left(J_0^2 \cdot \delta F_s\right)^\dagger - \phi\right) F_{\mathrm{eq},s}\mathcal{J}_s \mathrm{d}v_\parallel \mathrm{d}\mu_s = 0, \quad (41)$$

where the first term is the perturbed gyrocenter charge density and the second is the polarization density which is only calculated from the local Maxwellian. In this expression, J_0 is the gyroaverage operator and the dagger symbol represents its complex conjugate. Similarly, the parallel vector potential is calculated from parallel Ampère's law,

$$-\nabla^2 A_\parallel + \sum_s \frac{\mu_0 Z_s^2 e^2}{T_s}\int v_\parallel^2 \left(J_0^2 \cdot A_\parallel\right)^\dagger F_{\mathrm{eq},s}\mathcal{J}_s \mathrm{d}v_\parallel \mathrm{d}\mu_s$$
$$= \sum_s \frac{\mu_0 Z_s e}{T_s}\int v_\parallel (J_0 \cdot g_s)^\dagger \mathcal{J}_s \mathrm{d}v_\parallel \mathrm{d}\mu_s. \quad (42)$$

B. Simulation set-up to analyze the tearing instability in GKW

The tearing mode is linearly excited in the code[21] by introducing an electron flow u_e in the equilibrium distribution function. The generated tearing mode is driven due to the inertia of electrons when we neglect resistivity through collisions. The mean velocity of electrons is related to the imposed q profile following the expression (21). We use the same q profile as for our analytical calculations, given by Eq. (27). As an example, a linear collisionless simulation of a self-consistent tearing mode has been run for the following parameters: aspect ratio $R_0/a = 3.33$, normalized ion Larmor radius $\rho_\star = \rho_i/R_0 = 0.002815$, safety factor at the edge $q_a = 3.5$, and current peaking parameter $\nu = 2.6$. This corresponds to a tearing mode with $\Delta' \approx 17.31$, calculated using the shooting method to solve the tearing equation outside the resonant layer, as presented in Sec. III A. We represent in Fig. 3 the safety factor profile described by Eq. (27) (bottom) for these parameters, the radial eigenfunction of the parallel vector potential (middle), and its second radial derivative (top), which is highly localized around the resonant layer at the $q(r/R_0) = 2$ surface, represented by a vertical dashed line together with the label $r = r_s$. For linear simulations, a single $n = 1$ toroidal mode is considered and the numerical resolution is $N_r \times N_s \times N_{v_\parallel} \times N_\mu = 512 \times 30 \times 64 \times 15$, where N_r is the number of radial grid points, N_s is the number of points in the parallel direction, $N_{v_\parallel}$ is the number of points in parallel velocity, and N_μ is the number of points in the magnetic moment direction. The selected number of points in the radial direction is enough to describe the physics around the thin resonant layer.[21] In our collisionless simulations, we can artificially suppress the electrostatic potential, the mirror term, and the curvature of the magnetic field. This capability allows us to run the code in the same limit as the one where the analytical theory has been derived. When radial gradients are used in the simulations, the reference position r_0 is the same as the position of the resonant surface, i.e., $r_0 = r_s$, and the width of the region where the gradient is localized is set to $w = 0.03$.

C. Parametric study of the collisionless tearing mode

Analytically, we have shown previously that, when particle trapping is taken into account, the growth rate is increased by a factor $1 + 2\epsilon$. The position of the resonant surface is inversely proportional to Δ'. This means that including trapping effects will amplify the growth rate by an ~ 1.44 factor that should decrease with Δ'. In Fig. 4, we represent the ratio between the tearing mode growth rate with and without trapping as a function of the stability parameter Δ', calculated using the shooting method and the q profile used in GKW. The scan on
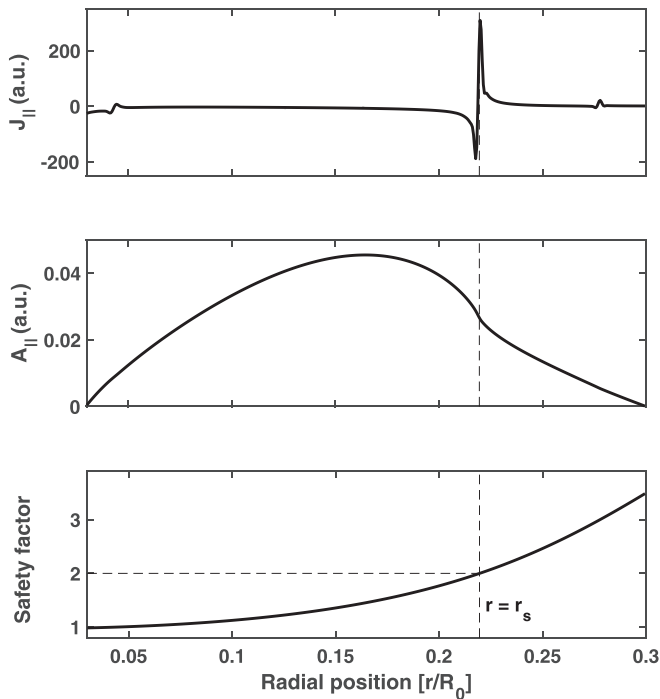
FIG. 3. The radial profiles of the imposed safety factor q (bottom), the parallel vector potential (middle), and its radial second derivative (top) as calculated by GKW in toroidal geometry for density and temperature gradients $R/L_n = R/L_T = 2.2$. The most unstable mode is located at the $q = 2$ surface, indicated by a vertical dashed line and labeled by $r = r_s$, where the parallel current is highly localized.

Δ' has been performed by changing the q_a and ν parameters in the q profile. The points used in this scan are indicated by asterisks in Fig. 2. The analytical prediction in dashed red line agrees with the numerical calculation from GKW simulations, represented by the solid black line, within an error of $\sim 1 - 5\%$. All the simulations used for Fig. 4 have been run by switching off the term $\mathbf{v}_D \cdot \nabla$ in the gyrokinetic equation,
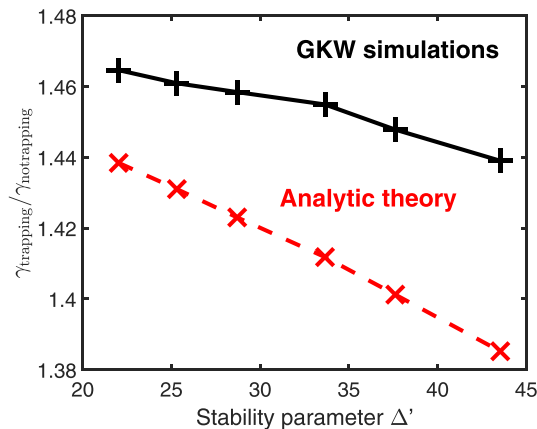
FIG. 4. The ratio between the growth rate with and without trapping in terms of Δ', shown by the solid black line as calculated numerically with GKW and by the red dashed line as predicted by our analytical theory.

which represents the magnetic gradient and curvature drift. This term can be switched on and off in the code independently of the mirror term $\mathbf{b} \cdot \nabla B$, responsible for the trapping of particles. This mirror term is the one that has been switched on and off to obtain the ratio $\gamma_{\text{trapping}}/\gamma_{\text{notrapping}}$. One can conclude that in the absence of magnetic drift, magnetic trapping due to the mirror term destabilizes the mode by a factor that depends on the position of the resonant surface of the mode.

We have subsequently performed a parametric study of the linear instability of the tearing mode to further study the impact of the curvature, radial gradients, and particle trapping. For this purpose, we have run a set of global simulations, with and without the temperature gradient, with and without particle trapping, and with and without the magnetic curvature. Note that the density gradient is always set to $R/L_n = 0$. This is due to the fact that the equilibrium parallel current depends linearly on the density. Therefore, in the absence of the density gradient, the stability parameter Δ' is not modified.

The growth rate in the absence of the temperature gradient is presented in Fig. 5. The calculated growth rate is plotted as a function of Δ' in the left panel and $|k'_{\parallel}|\Delta'$ in the right panel. The black curves represent the case of no particle trapping, neglecting (solid) and taking into account (dashed) the curvature of the magnetic field. These curves are conveniently labeled in the figure. For the sake of readability, the same labels, colors, and symbols are used in the following. As predicted by theory, in the absence of particle trapping, the two curves with/without the magnetic curvature overlap in the case of flat density and temperature profiles. When the mirror term $\mathbf{b} \cdot \nabla B$ inducing magnetic trapping is considered, the collisionless tearing mode is more unstable, which is consistent with Fig. 4. In that case, it is observed that adding the magnetic drift $\mathbf{v}_D \cdot \nabla$ stabilizes the mode. The reason for this effect is analyzed in Sec. VI B.

Regarding the dependence on the stability parameter, our analytical theory predicts a linear scaling of the growth rate with Δ', regardless of the pressure profile. We observe that the trend of the curve with Δ' is linear only for small values of Δ' and departs from the linear behavior when increasing Δ'. Actually, when modifying Δ', the position of the resonant surface is also modified and so is the value of $|k'_{\parallel}|$, which implies that the proportionality coefficient is modified. However, when looking at the dependence of the growth rate on $|k'_{\parallel}|\Delta'$, a linear behavior is observed, which is in better agreement with the analytical relation found in Sec. IV.

Note, nonetheless, that a nonlinear behavior of the growth rate was reported in Ref. 36, where the growth rate was found to scale as $\sqrt{\Delta'}$. This behavior was explained by the short wavelength effects taken into account in the Bessel function $J_0(k_{\perp}\rho_e)$. The Bessel function was then expanded for large arguments, and a scaling of the growth rate with $\sqrt{\Delta'}$ and $(\rho_e a)^{1/4}$ was found. The latter is a finite Larmor radius effect. However, when we eliminate the finite Larmor radius effect in the code, by not computing the gyroaverage, we have not observed any change in the growth rate of the mode. The effect of variations of the wave vector in the radial direction cannot be verified *per se* in our simulations since a Fourier representation is used for the binormal coordinate (perpendicular to the field) and we consider only one binormal mode. One would need to consider more than a single mode to check this effect, which is left for a future publication.

When the temperature gradient is included, the growth rate is amplified with respect to the case $R/L_T = 0$ only when considering
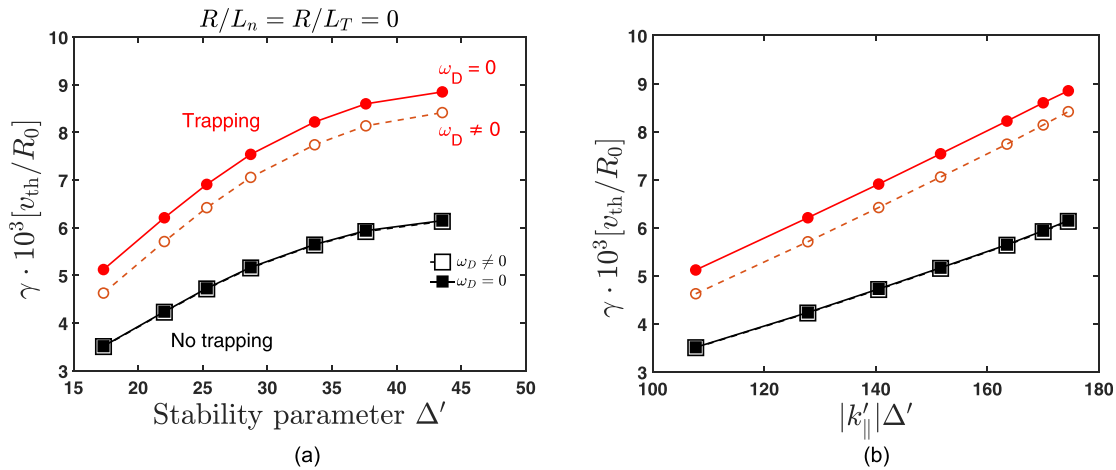
FIG. 5. The growth rate of a collisionless tearing mode for flat background profiles as a function of Δ' (left) and $|k'_\|\|\Delta'$ (right) given by Gᴋᴡ simulations, for several cases of a population consisting of only passing particles and passing and trapped particles and neglecting/considering magnetic drift.

the particle trapping, which is in agreement with analytical calculations.[24] Note that the opposite result can be obtained in different regimes, as was found in δF PIC gyrokinetic simulations in the slab geometry limit,[23] where the temperature gradient tends to stabilize the tearing mode. In order to make quantitative comparisons between our results and those of Ref. 23, we should perform further simulations in slab geometry, which is beyond the scope of the present paper. If particle trapping is neglected, the impact of the temperature gradient is negligible. This is shown in Fig. 6, where the dependence of the growth rate on the stability parameter Δ' is plotted considering a temperature gradient $R/L_T = 6.9$. It is observed that the effect of the magnetic drift frequency is opposite to that in the absence of the temperature gradient, i.e., the magnetic curvature tends to destabilize the collisionless tearing mode. This is in agreement with recent analytical results based

on a fluid approach,[37] which suggests an interchangelike destabilization of the collisionless tearing mode, i.e., a destabilization due to the temperature gradient when the magnetic curvature is taken into account. Nevertheless, further quantitative analysis for comparison between fluid and gyrokinetic theories should be done, which is beyond the scope of the present paper.

We have seen that, in the presence of particle trapping, for $R/L_T = 0$ ($R/L_T = 6.9$, respectively), the magnetic curvature stabilizes (destabilizes, respectively) the mode. This implies that there must exist a temperature gradient at which the interchange destabilization[37] compensates for the stabilization observed in Fig. 5. To analyze this more in detail, we have selected one single Δ' and we have performed a scan on the temperature gradient R/L_T. The result is shown in Fig. 7. It is observed that, when neglecting the particle trapping, the temperature gradient does not have any significant impact on the
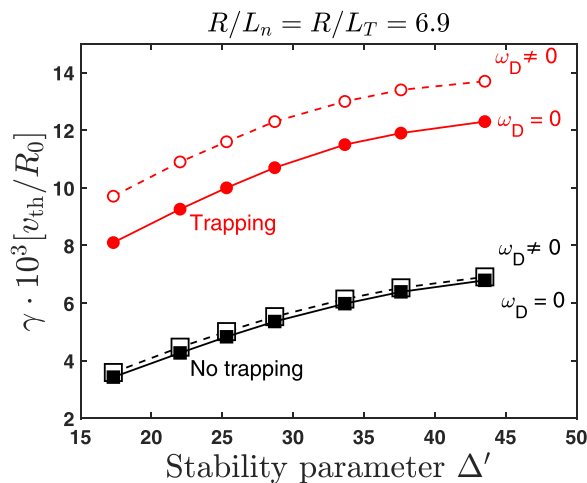

FIG. 6. The growth rate of a collisionless tearing mode for a flat density gradient and a nonzero temperature gradient ($R/L_T = 6.9$) as a function of Δ' given by Gᴋᴡ simulations, for several cases of a population consisting of only passing particles and passing and trapped particles and neglecting/considering magnetic drift.
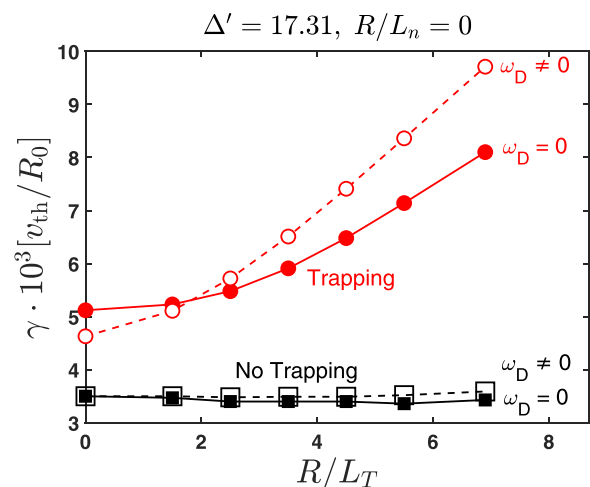

FIG. 7. The growth rate of a collisionless tearing mode as a function of R/L_T for a flat density profile and fixed Δ'.

tearing mode stability. However, when some particles are trapped, the temperature gradient destabilizes the mode. This destabilization is further increased by the magnetic field curvature only beyond an R/L_T-threshold around $R/L_T \approx 2$.

For the sake of completeness, we have run simulations with flat density and temperature profiles, but considering the electrostatic potential by solving the quasineutrality equation, coupled to the gyro-kinetic Vlasov-Ampère system. We show the results in Fig. 8. We confirm that including trapping effects destabilizes the mode even in the presence of electrostatic potential. We also confirm a stabilizing role in the curvature in the case of zero gradients, even when the destabilizing effect[38] of the electrostatic potential is considered.

We can see that the role of the magnetic field curvature in particle trapping is to stabilize the mode when no gradients are considered and to destabilize it when temperature gradients are considered, beyond an R/L_T-threshold. This threshold occurs when a stabilizing effect due to trapped particles is compensated by the interchange destabilization. To get a better understanding of the underlying physics, a quantitative analysis of the energy exchange between the particles and the mode has been made by using diagnostics that computes the variation of the kinetic energy of particles in the code.

VI. ENERGY EXCHANGE DIAGNOSTICS FOR WAVE-PARTICLE INTERACTION

The following diagnostics is used to identify in velocity space the various contributions of passing and trapped particles to the linear growth rate of the most unstable mode. Note that in our case, we focus on the interaction between the tearing mode and electrons. The diagnostics is based on the energy conservation property of the Vlasov-Poisson system of equations, which allows us to directly link the mode growth rate to the work done by the perturbed electric field on the particles. Strictly speaking, this method is only applicable if the set of equations is solved and their numerical implementation conserves energy.
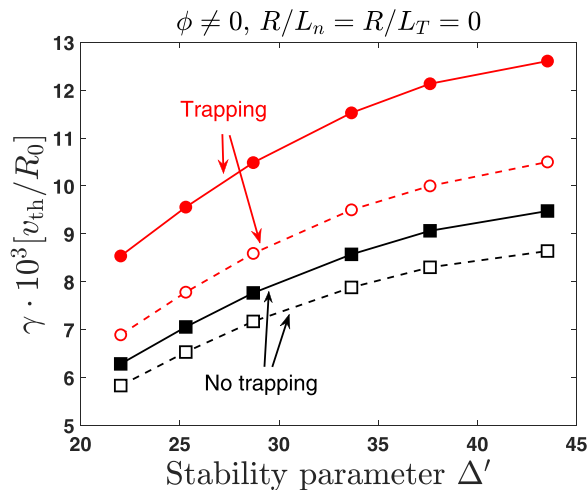
FIG. 8. The growth rate of a collisionless tearing mode as a function of Δ' for flat temperature and density profiles, but considering the electrostatic potential ($\phi \neq 0$).

A. Conservation of energy

The time variation of the space-integrated potential energy of an electromagnetic wave is given by

$$\frac{d\mathcal{E}_p}{dt} = \frac{d}{dt}\int d^3\mathbf{x}\left(\frac{\epsilon_0}{2}\mathbf{E}\cdot\mathbf{E} + \frac{\epsilon_0 c^2}{2}\mathbf{B}\cdot\mathbf{B}\right)$$
$$= \int d^3\mathbf{x}\left(\epsilon_0\mathbf{E}\cdot\frac{\partial\mathbf{E}}{\partial t} + \epsilon c^2\mathbf{B}\cdot\frac{\partial\mathbf{B}}{\partial t}\right). \quad (43)$$

Using Faraday's induction law $\nabla\times\mathbf{E} = -\partial_t\mathbf{B}$ and Ampère's law $\nabla\times\mathbf{B} = \mu_0\mathbf{J} + \mu_0\epsilon_0\partial_t\mathbf{E}$, where $\mathbf{E}$, $\mathbf{B}$, and $\mathbf{J}$ are the electric field, the magnetic field, and the current density, respectively, Eq. (43) becomes

$$\frac{d\mathcal{E}_p}{dt} = -\int d^3\mathbf{x}\left[\mathbf{J}\cdot\mathbf{E} + \frac{1}{\mu_0}\nabla\cdot(\mathbf{E}\times\mathbf{B})\right]. \quad (44)$$

Owing to the conservation of the total energy of the system, we have

$$\frac{d\mathcal{E}_k}{dt} = -\frac{d\mathcal{E}_p}{dt}, \quad (45)$$

where $\mathcal{E}_k$ is the kinetic energy of particles. This gives the time evolution of the kinetic energy

$$\frac{d\mathcal{E}_k}{dt} = -\sum_s\int d^3\mathbf{x}\,d^3\mathbf{v}\,Z_s e\,F_s\,\mathbf{v}\cdot\left(\nabla\tilde{\phi}\phi + \frac{\partial\tilde{\phi}A_\parallel}{\partial t}\mathbf{b}\right)$$
$$+ \int d^3\mathbf{x}\,\frac{1}{\mu_0}\nabla\cdot(\mathbf{E}\times\mathbf{B}). \quad (46)$$

The sign of the time evolution of the kinetic energy indicates the contribution to the growth rate of the mode. If $\dot{\mathcal{E}}_k > 0$, the energy is transferred from the mode to the particles, and therefore, the mode is damped. In the opposite case, the mode gains energy and is therefore unstable. It is important to note that in the case of global modes such as tearing modes, a positive variation of the particles' kinetic energy at a local point does not necessarily suggest destabilization of the whole mode. Some transport of energy should be taken into account through advection, especially when the electrostatic potential is considered and the $\nabla\cdot(\mathbf{E}\times\mathbf{B})$ term is nonzero. In our simulations, we check that even when the electrostatic potential is taken into account that term is negligible compared to the $\mathbf{J}\cdot\mathbf{E}$ term. We have implemented in the code the first term on the right hand-side of Eq. (46) as a function of $(r, v_\parallel, v_\perp)$. The last term on the right-hand side is calculated in separate diagnostics that computes all the radial flows. The implemented diagnostics reads

$$\dot{\mathcal{E}}_k = -eZ_s\int d\ell F\left(v_\parallel\mathbf{b} + \mathbf{v_E} + \mathbf{v_D}\right)\cdot\left(\nabla J_0\cdot\phi + \partial_t J_0\cdot A_\parallel\mathbf{b}\right), \quad (47)$$

with ℓ being the parallel coordinate.

B. Response of the particles to the tearing mode

We present the results from the described diagnostics, which allows us to characterize the particle response to the collisionless tearing instability in the purely magnetic case, i.e., the electrostatic potential is set to zero, and therefore, the $\mathbf{E}\times\mathbf{B}$ flux in Eq. (46) vanishes. The local interaction between the waves and particles in the velocity space can thus be described by Eq. (47) with the $A_\parallel$ term only.

Figure 9 illustrates the local exchange of energy between particles and the mode in the velocity space for $R/L_n = R/L_T = 0$. Positive (negative, respectively) values imply a transfer of energy from the mode to the particles (from the particles to the mode, respectively). The plots are shown for a local point around the resonant position $r = r_s$, where the exchange of energy is the most localized. The dashed line in the middle panel denotes the trapping cone $v_\parallel = \sqrt{2r_s/R_0}v_\perp$. As discussed earlier, this relation is valid only at the tokamak midplane, where the magnetic field intensity has a maximum value. Therefore, one needs to be aware of the position on the magnetic field when setting the trapping boundary. In our simulations, the amplitude of the mode is localized at $l = 0$, which makes this relation valid. The three different panels represent the three different curves that we have shown in Fig. 5 (actually, we have four curves, but when there is no particle trapping, the two black curves are the same). It is observed that when trapping is considered without the magnetic curvature, the effect is the suppression of the particle response inside the trapping cone, as predicted by our analytical theory. Numerical integration in velocity space results in a reduction of 13% of the integrated values of $\dot{\mathcal{E}}_k$ in Fig. 9(b) with respect to Fig. 9(a). Although quantitative analysis to compare with the modification of the growth rate would also require integration over the radial position, the result we obtain is

qualitatively consistent with a reduced local transfer of energy from the mode to the particles. Let us remind that the tearing mode gets the energy from the outer region (represented by Δ') and transfers part of this energy to particles in the resonant layer. Therefore, the fact that the tearing mode transfers less energy to the particles in the resonant layer implies that there is more energy available for the mode, which results in an increased growth rate. However, when including the magnetic curvature and trapping is allowed, trapped particles respond to the presence of the tearing mode, allowing in this way the transfer of energy from the tearing mode to the trapped particles, which results in a decrease in the growth rate. This is evidenced by Fig. 9(c), where the red curve represents the positions in velocity space at the resonant surface where the precession frequency of trapped particles equals the tearing frequency, i.e., $\omega = n_3 \Omega_3(v_\parallel, v_\perp)$, with $n_3 = 1$. The frequencies of motion are calculated in detail in Appendix C. In particular, we use expression C30 to plot the red curve. It is observed that the maximum of the response is located on the red curve and corresponds to barely trapped particles. Consequently, one can assess that adding particle trapping in the presence of the magnetic curvature can modify the stability of the mode through the resonance between the tearing mode and barely trapped particles.
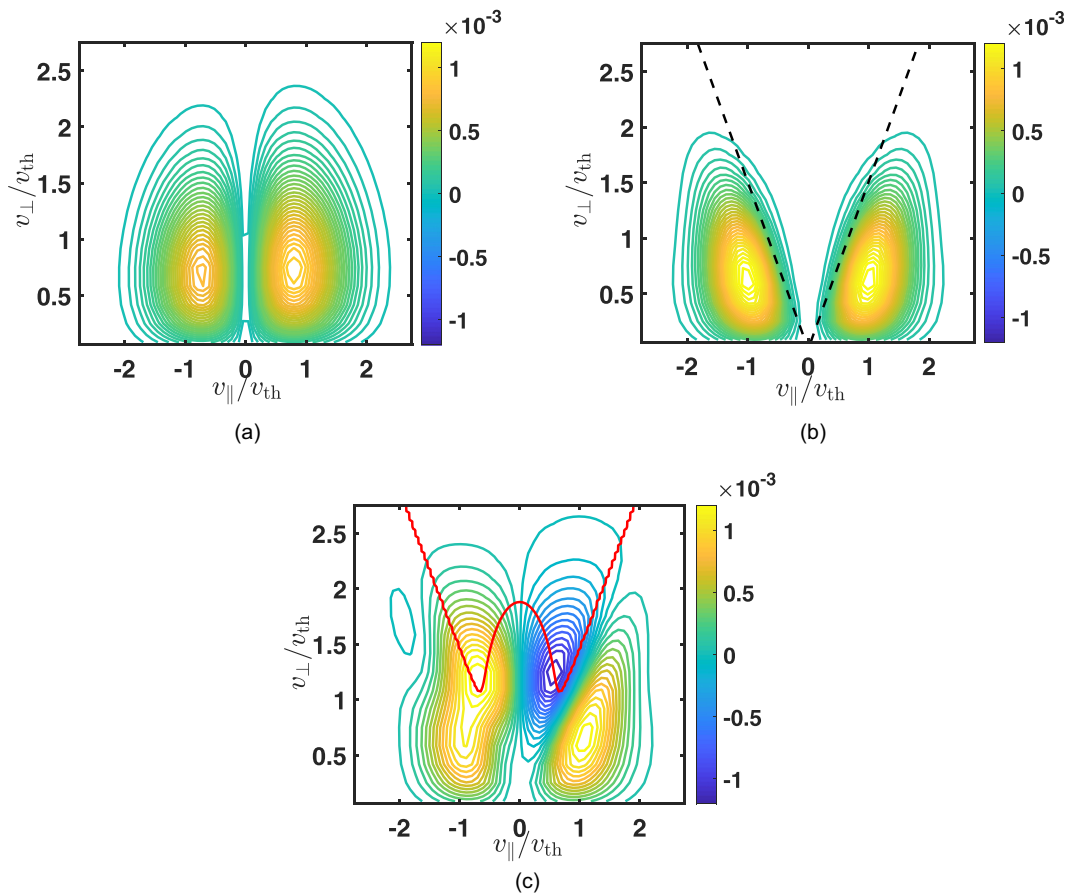
FIG. 9. Time derivative of the kinetic energy at the resonant position in the presence of a collisionless tearing mode without density/temperature gradients, i.e., $R/L_n = R/L_T = 0$. (a) Without particle trapping. (b) With particle trapping and $\omega_D = 0$. (c) With particle trapping and $\omega_D \neq 0$.

VII. CONCLUSIONS

In this paper, we have studied the stability of a collisionless tearing mode in a curved and inhomogeneous magnetic field. The tearing mode equation is derived in the framework of gyrokinetic theory using a Hamiltonian approach. The dispersion equation was obtained for the tearing instability, describing both the outer (ideal or nonresonant) and inner (nonideal or resonant) regions. Using the gyrokinetic theory in the analysis of the tearing mode allows us to look into the kinetic aspects of the instability and therefore analyze possible resonances between particles and the mode in the inner region. In the outer region, the fluid limit is used to avoid the resonances. A shooting method has been employed to integrate the equation of the tearing mode for a general safety factor profile, and a diagram of the stability parameter Δ' has been obtained.

We have solved analytically the equation of the tearing mode in the inner region, where the kinetic effects are kept, and we have recovered the result that the growth rate scales linearly with $|k'_\parallel|\Delta'$, where $k'_\parallel$ is the radial derivative of the parallel wave-vector evaluated at the resonant surface. We have also found that trapping effects in the absence of magnetic curvature lead to an increase in the growth rate by a factor $1 + 2\epsilon$, where $\epsilon = r/R_0$. This is due to the fact that the mode transfers its energy mainly to passing electrons in the resonant layer. Therefore, introducing trapped electrons increases the energy available for the mode to grow. Moreover, we have predicted that the magnetic field curvature does not play any role in the stability of the tearing mode when only passing electrons are considered.

Further analysis has been carried out numerically, by means of linear global gyrokinetic simulations using GKW code. We have verified our analytical results, namely, the linear scaling of the growth rate with $|k'_\parallel|\Delta'$ and the destabilization due to trapped electrons. We have subsequently performed a parametric study of the stability of the tearing mode, and we have obtained two main results. First, in the presence of trapped particles, the temperature gradient plays a destabilizing role. Second, we have reported that the magnetic field curvature tends to further destabilize the mode in combination with the temperature gradient, suggesting a destabilization through an interchange mechanism.[37] We have shown that there exists a threshold in temperature gradient below which the magnetic curvature is stabilizing. We have identified a response of trapped particles to the tearing mode, which results in a kinetic damping of the mode. The threshold in the temperature gradient appears when this kinetic damping is balanced by the interchange destabilization due to the combination of the temperature gradient and the magnetic field curvature. These findings open the way to a deeper understanding of the tearing instability in tokamaks in the presence of kinetic effects and shed light on the dependence of its growth rate on a set of tokamak control parameters.

ACKNOWLEDGMENTS

APPENDIX A: EXACT LINEAR SOLUTION OF THE GYROKINETIC EQUATION

The starting point to obtain the linear response of electrons is the Vlasov equation in conservative form using a Hamiltonian formalism,

$$\frac{\partial F}{\partial t} - [\mathcal{H}, F] = 0. \tag{A1}$$

Here, $[X, Y]$ represents the Poisson brackets between X and Y, i.e., $[X, Y] = \partial_\mathbf{x} X \partial_\mathbf{p} Y - \partial_\mathbf{p} X \partial_\mathbf{x} Y$, where $\mathbf{x}$ and $\mathbf{p}$ are the position and momenta, forming a set of canonical variables satisfying Hamilton's equations.

The calculation is performed in the so-called δF-approximation. For this purpose, we decompose the distribution function and the Hamiltonian into equilibrium and perturbed parts,

$$F = F_{\mathrm{eq}} + \delta F \tag{A2}$$

and

$$\mathcal{H} = \mathcal{H}_{\mathrm{eq}} + \delta\mathcal{H}, \tag{A3}$$

respectively, and assume the ordering $|\delta F|/F_{\mathrm{eq}} \approx \rho_\star$ and $|\delta\mathcal{H}|/|\mathcal{H}_{\mathrm{eq}}| \approx \rho_\star$. Vlasov equation (A1) for electrons is then linearized and written for δF as

$$\frac{\partial \delta F}{\partial t} - [\mathcal{H}_{\mathrm{eq}}, \delta F] - [\delta\mathcal{H}, F_{\mathrm{eq}}] = 0. \tag{A4}$$

The equilibrium Hamiltonian is given by

$$\mathcal{H}_{\mathrm{eq}} = \frac{|\mathbf{p} - eZ_e\mathbf{A}_{\mathrm{eq}}|^2}{2m_e} + eZ_e\phi_{\mathrm{eq}}, \tag{A5}$$

where $\mathbf{A}_{\mathrm{eq}}$ and ϕ_{eq} are the equilibrium vector and electrostatic potentials, respectively, $\mathbf{p} = m_e\mathbf{v} + eZ_e\mathbf{A}$ is the electron momentum, and Z_e is the atomic number of the species, which is $Z_e = -1$ in this particular case where only electrons are considered. The perturbed Hamiltonian is written in terms of the perturbed vector and electrostatic potentials, $A_\parallel$ and ϕ, respectively, as

$$\delta\mathcal{H} = eZ_e(\phi - v_{\parallel,\mathrm{eq}}A_\parallel), \tag{A6}$$

where $v_{\parallel,\mathrm{eq}}$ is the projection of the electron velocity onto the unperturbed magnetic field lines. This formulation can lead to simple insightful equations of motion when expressed in canonical variables $(\mathbf{x}, \mathbf{p})$. However, the periodicity of particle motion in a tokamak suggests the use of a different set of canonically conjugated variables, called action-angle variables and represented by $\mathbf{J} = (J_1, J_2, J_3)$ and $\boldsymbol{\alpha} = (\alpha_1, \alpha_2, \alpha_3)$. These angles describe the gyromotion (α_1), the

motion in the poloidal direction (α_2), and the motion in the toroidal direction (α_3). The equations of motion using these coordinates can be written as

$$\dot{\boldsymbol{\alpha}} = \frac{\partial \mathcal{H}_{eq}}{\partial \mathbf{J}} = \boldsymbol{\Omega}_{eq}(\mathbf{J}) \quad \dot{\mathbf{J}} = -\frac{\partial \mathcal{H}_{eq}}{\partial \boldsymbol{\alpha}}, \quad (A7)$$

where the angles are supposed to vary linearly in time giving the characteristic frequencies of motion at equilibrium $\boldsymbol{\Omega} = (\Omega_1, \Omega_2, \Omega_3)$. For completeness, these frequencies are derived in detail in Appendix C.

We define an equilibrium quantity X_{eq} as the average of the quantity X over the angles $\boldsymbol{\alpha}$, i.e.,

$$X_{eq} \equiv \int d^3\boldsymbol{\alpha}\, X, \quad (A8)$$

which means that the only dependence of X_{eq} is on the actions $\mathbf{J}$, i.e., $X_{eq} = X_{eq}(\mathbf{J})$. The equilibrium distribution function and the equilibrium Hamiltonian are therefore functions of the motion invariants, and the perturbed distribution function and Hamiltonian are functions of $(\boldsymbol{\alpha}, \mathbf{J}, t)$. Following this definition, the equations of motion (A7) introduce the actions as motion invariants, i.e., $\dot{\mathbf{J}} = \mathbf{0}$. Therefore, without any loss of generality, any equilibrium quantity can be defined as a function of the motion invariants associated with the three directions of periodicity.

The periodicity of the perturbed quantities with respect to the angles $\boldsymbol{\alpha}$ allows us to perform a Fourier expansion,

$$\begin{Bmatrix} \delta \mathcal{H} \\ \delta F \end{Bmatrix}(\boldsymbol{\alpha}, \mathbf{J}, t) = \sum_{\mathbf{n}\omega} \begin{Bmatrix} \delta \mathcal{H}_{\mathbf{n}\omega} \\ \delta F_{\mathbf{n}\omega} \end{Bmatrix}(\mathbf{J}) \exp\left[i(\mathbf{n} \cdot \boldsymbol{\alpha} - \omega t)\right], \quad (A9)$$

where $\mathbf{n} = (n_1, n_2, n_3)$ are the wave numbers associated with the angles $\boldsymbol{\alpha} = (\alpha_1, \alpha_2, \alpha_3)$ and ω is the frequency of the tearing mode. Substituting Eq. (A9) into the linearized Vlasov equation (A4) and using the equations of motion (A7), an exact linear solution can be found,

$$\delta F_{\mathbf{n},\omega} = -\frac{\mathbf{n} \cdot \partial_{\mathbf{J}} F_{eq}}{\omega - \mathbf{n} \cdot \boldsymbol{\Omega}}\, \delta \mathcal{H}_{\mathbf{n},\omega}. \quad (A10)$$

In the adiabatic limit, the first motion invariant is proportional to the magnetic moment $\mu = m_e v_\perp^2/(2B)$, i.e., $J_1 = m_e \mu/(eZ_e)$. The second action, J_2, is written in terms of the toroidal flux of the magnetic field Φ as $J_2 = eZ_e\Phi + \frac{1}{2\pi}\oint m_e v_\parallel d\ell$, where ℓ is the coordinate along the magnetic field line and $v_\parallel$ is the component of the guiding-center velocity parallel to the magnetic field. Finally, the third action J_3 is the toroidal canonical momentum $J_3 \equiv P_\varphi = -eZ_e\psi + m_e R v_\varphi$, with ψ being the poloidal flux of the magnetic field, R being the major radius, and v_φ being the projection of the electron velocity onto the toroidal direction. For highly passing electrons, the second action is closer to a radial function than J_3 is. Therefore, changing the variable $\mathbf{J} \to \mathbf{I}$, where $\mathbf{I} = (J_1, J_2, \mathcal{H}_{eq})$, makes it possible to introduce radial gradients of the equilibrium. This change in variable introduces the equilibrium Hamiltonian, i.e., the energy in the absence of any perturbation, which is more convenient for physical analysis. The numerator of Eq. (A10) can therefore be written as follows:

$$\mathbf{n} \cdot \partial_{\mathbf{J}} F_{eq} = \mathbf{n} \cdot \frac{\partial \mathbf{I}}{\partial \mathbf{J}} \cdot \frac{\partial F_{eq}}{\partial \mathbf{I}} = n_1 \frac{\partial F_{eq}}{\partial J_1} + \mathbf{n} \cdot \boldsymbol{\Omega}\frac{\partial F_{eq}}{\partial \mathcal{H}_{eq}} + n_2 \frac{\partial F_{eq}}{\partial J_2}. \quad (A11)$$

We can now consider that $\Omega_1 \gg \omega, \Omega_2, \Omega_3$. This ordering yields the exact linear response to be used in the following:

$$\delta F_{\mathbf{n},\omega} = \frac{\partial F_{eq}}{\partial \mathcal{H}_{eq}}\delta \mathcal{H}_{\mathbf{n},\omega} + \frac{1}{B}\frac{\partial F_{eq}}{\partial \mu}\delta \mathcal{H}_{\mathbf{n}',\omega}$$
$$- \frac{\omega \partial_{\mathcal{H}_{eq}} F_{eq} + n_2 \partial_{J_2} F_{eq}}{\omega - \mathbf{n}^\star \cdot \boldsymbol{\Omega}}\delta \mathcal{H}_{\mathbf{n}^\star,\omega}, \quad (A12)$$

where $\mathbf{n}' = (n_1 \neq 0, n_2, n_3)$ and $\mathbf{n}^\star = (n_1 = 0, n_2, n_3)$.

APPENDIX B: PERTURBED PARALLEL CURRENT

The perturbed parallel current is calculated as

$$j_\parallel = eZ_e \int d^3\mathbf{p}\left(v_{\parallel,eq}\delta F + \delta v_\parallel F_{eq}\right), \quad (B1)$$

where the perturbed parallel velocity is expressed in terms of the parallel vector potential,

$$\delta v_\parallel = -\frac{eZ_e}{m_e}A_\parallel. \quad (B2)$$

Therefore, the perturbed parallel current reads

$$j_\parallel = eZ_e \int d^3\mathbf{p}\left(v_{\parallel,eq}\delta F - \frac{eZ_e}{m_e}A_\parallel F_{eq}\right). \quad (B3)$$

Passing from $(\mathbf{x}, \mathbf{p})$ to action-angle variables $(\boldsymbol{\alpha}, \mathbf{J})$ at this point requires to pass from a three-dimensional to a six-dimensional space. For this purpose, we use the δ-Dirac function such that $j_\parallel$ for electrons is calculated as a 6D integration,

$$j_\parallel(\mathbf{x}, t) = eZ_e \int d^3\mathbf{p}d^3\mathbf{x}'\, \delta(\mathbf{x}' - \mathbf{x})\left(v_{\parallel,eq}\delta F - \frac{eZ_e}{m_e}A_\parallel F_{eq}\right), \quad (B4)$$

where $\mathbf{x}'$ is a spatial position for the integration. We can now make the canonical change in variable $(\mathbf{x}, \mathbf{p}) \to (\boldsymbol{\alpha}, \mathbf{J})$, which gives

$$j_\parallel(\mathbf{x}, t) = eZ_e \int d\tau^\star d\alpha_1 \delta(\mathbf{x}' - \mathbf{x})\left(v_{\parallel,eq}\delta F - \frac{eZ_e}{m_e}A_\parallel F_{eq}\right), \quad (B5)$$

where we have separated the integration variables into gyrophase $d\alpha_1 \equiv d\varphi_c$ and $d\tau^\star = d\alpha_2\, d\alpha_3\, dJ_1\, dJ_2\, dJ_3$. We make use of Parseval's identity for Fourier series,

$$\int \frac{d\alpha_1}{2\pi}\delta(\mathbf{x}' - \mathbf{x})\delta F = \sum_{n_1} \left[\delta(\mathbf{x}' - \mathbf{x})\right]_{n_1} \delta F_{n_1}^\dagger, \quad (B6)$$

where $\dagger$ designates the complex conjugate of the perturbed quantity. The n_1 mode of the Dirac function can be calculated using the definition of the Dirac distribution,

$$\left[\delta(\mathbf{x}' - \mathbf{x})\right]_{n_1} = \int \frac{d\alpha_1}{2\pi}\delta(\mathbf{x}' - \mathbf{x})e^{-in_1\alpha_1}$$
$$= \int \frac{d\alpha_1}{2\pi}\int \frac{d^3\mathbf{k}}{(2\pi)^3}\, e^{i\mathbf{k}\cdot\mathbf{x}' - i\mathbf{k}\cdot\mathbf{x}}e^{-in_1\alpha_1}. \quad (B7)$$

Therefore, the parallel current density in Eq. (B5) can be expressed using the Bessel function of the first kind, defined as $\int d\alpha_1/(2\pi)\, ; e^{i(k_\perp \rho_c \cos\alpha_1 - n_1\alpha_1)} = (-i)^{n_1}J_{n_1}(k_\perp \rho_c)$,

$$j_\parallel(\mathbf{x}, t) = eZ_e \int \mathrm{d}\tau^\star \sum_{n_1} (-i)^{n_1} \int \frac{\mathrm{d}^3\mathbf{k}}{(2\pi)^3} \mathrm{e}^{i\mathbf{k}\cdot(\mathbf{x}_G - \mathbf{x})} J_{n_1}(k_\perp \rho_c)$$
$$\times \left(v_{\parallel,eq} \delta F_{n_1}^\dagger - \frac{eZ_e}{m_e} A_{\parallel n_1}^\dagger F_{eq} \right). \tag{B8}$$

Here, the perturbed quantities are functions of $(\mathbf{x}_G, \mathcal{H}_{eq}, P_\varphi)$. Note that through this Hamiltonian formalism, one can obtain the parallel current associated with the particle motion, in terms of particle coordinates $\mathbf{x}$, using physical quantities describing the guiding-center motion, which depends on guiding-center coordinates $\mathbf{x}_G$. Similarly, we calculate the n_1-mode of each component of δF and we substitute it into the expression of the parallel current in Eq. (B8). Anticipating the fact that we will later use the deeply passing particle approximations, we pass to an integration in guiding center coordinates $\mathrm{d}\tau^\star = \mathrm{d}\alpha_2\, \mathrm{d}\alpha_3\, \mathrm{d}J_1\, \mathrm{d}J_2\, \mathrm{d}J_3 \to \mathcal{J}\mathrm{d}\mathbf{x}_G\, \mathrm{d}v_{\parallel,eq} v_\perp \mathrm{d}v_\perp$, where $\mathcal{J}$ is the Jacobian of the transformation. We again now make use of the ordering $\Omega_1 \gg \omega, \Omega_2, \Omega_3$, which implies that the third term in the right-hand side of Eq. (4) is negligible except for $n_1 = 0$. Therefore, we keep only the $n_1 = 0$ terms, which strictly speaking is exactly the same as performing a gyroaverage. Using the Bessel function property $\sum_{n=-\infty}^{+\infty} J_n^2(x) = 1$[34] and the inverse Fourier transform

$$\int \frac{\mathrm{d}^3\mathbf{k}}{(2\pi)^3} \delta\hat{\mathcal{H}}^\dagger(\mathbf{k}, t)\, \mathrm{e}^{-i\mathbf{k}\cdot\mathbf{x}} = \delta\mathcal{H}(\mathbf{x}, t), \tag{B9}$$

we obtain the following general expression for the parallel current in the gyrokinetic approach using the magnetic limit, i.e., neglecting the electrostatic potential:

$$j_\parallel(\mathbf{x}, t) = -e^2 \int \mathcal{J}\mathrm{d}v_{\parallel,eq}\mathrm{d}\mu \Bigg\{ v_{\parallel,eq}^2 \partial_{\mathcal{H}_{eq}} F_{eq} A_\parallel(\mathbf{x}, t)$$
$$+ v_{\parallel eq}^2 \frac{1}{B} \frac{\partial F_{eq}}{\partial \mu} \left(1 - J_0^2\right) A_\parallel(\mathbf{x}, t)$$
$$+ \sum_{n_2, n_3} v_{\parallel,eq}^2 \frac{\omega \partial_{\mathcal{H}_{eq}} F_{eq} + n_2 \partial_{J_2} F_{eq}}{\omega - n_2 \Omega_2 - n_3 \Omega_3} J_0^2 A_{\parallel n_2, n_3, \omega}(\mathbf{x})$$
$$\times \mathrm{e}^{i(n_2 \alpha_2 + n_3 \alpha_3 - \omega t)} + \frac{1}{m_e} F_{eq} A_\parallel(\mathbf{x}, t) \Bigg\}, \tag{B10}$$

where $J_0 \equiv J_0(k_\perp \rho_c)$, J_0^2 represents the gyroaverage operator applied twice, and the squared electron charge $Z_e^2 = 1$ has been removed for the sake of clarity. We choose the equilibrium distribution function,

$$F_{eq} = \frac{n_{eq}}{\left(2\pi T_{eq}/m_e\right)^{3/2}} \mathrm{e}^{-\frac{\mathcal{H}_{eq} - \mathcal{U}_{eq}}{T_{eq}}}, \tag{B11}$$

where n_{eq} and T_{eq} are the equilibrium density and temperature, respectively, and $\mathcal{U}_{eq}$ is a function which depends on the motion invariants. For our purpose, this function will be odd in $v_\parallel$, in order to generate an equilibrium parallel current. After integration, the first and last terms of the right-hand side in expression (B10) cancel out. For electrons, one can take the small orbit limit and approximate the Bessel function as $J_0^2(k_\perp \rho_c) \approx 1$ for $k_\perp \rho_c \ll 1$. Therefore, the second term with $\partial F_{eq}/\partial \mu$ vanishes. Finally, $j_\parallel(\mathbf{x}, t)$ is written as

$$j_\parallel(\mathbf{x}, t) = \frac{e^2}{T_{eq}} \sum_{n_2, n_3} \left\langle v_{\parallel,eq}^2 \frac{\omega - n_2 T_{eq} \partial_{J_2} \log F_{eq}}{\omega - n_2 \Omega_2 - n_3 \Omega_3} \right\rangle$$
$$\times A_{\parallel n_2, n_3, \omega}(\mathbf{x}) \mathrm{e}^{i(n_2 \alpha_2 + n_3 \alpha_3 - \omega t)}, \tag{B12}$$

where the notation $\langle \cdots \rangle$ has been used for simplicity to represent an average over gyrocenter equilibrium velocity space weighted by the equilibrium distribution function,

$$\langle \cdots \rangle = \int \mathcal{J}\mathrm{d}v_{\parallel,eq}\mathrm{d}\mu \cdots F_{eq}. \tag{B13}$$

If we restrict our analysis to deeply passing electrons, we can write $\alpha_2 = \theta$ and $\alpha_3 = \varphi$, where θ and φ are the poloidal and toroidal angles, respectively. Consequently, $n_2 = m$ and $n_3 = n$, with m and n being the poloidal and toroidal mode numbers, respectively. The frequencies Ω_2 and Ω_3 are calculated in detail in Appendix C. For deeply passing particles, these frequencies can be approximated as

$$\Omega_2 \approx \frac{v_{\parallel,eq}}{qR_0}, \tag{B14}$$

$$\Omega_3 \approx \frac{2q}{r} \frac{m_e v_{\parallel,eq}^2 + \mu B_0}{eZ_e B_0 R_0} + \frac{v_{\parallel,eq}}{R_0}, \tag{B15}$$

where q is the safety factor, which represents the helicity of the magnetic field lines, and r is the minor radius. B_0 and R_0 are the modulus of the magnetic field and the major radius, respectively, measured at the magnetic axis. The perturbed parallel current will be written in normalized units. For this purpose, we normalize the velocities to the thermal velocity of electrons v_{th}, the distances to R_0, the frequencies to the transit frequency $\omega_t = v_{th}/R_0$, the equilibrium distribution function to n_0/v_{th}^3, with n_0 some normalizing density, the parallel vector potential to $B_0 R_0 \rho_\star^2$, and the temperature to a normalizing temperature defined as $T_0 = m_e v_{th}^2/2$. The parallel current can then be rewritten as

$$j_\parallel(\mathbf{x}, t) = \rho_\star e n_0 v_{th} \frac{2}{\hat{T}_{eq}} \sum_{m, n, \omega} \left\langle \hat{v}_\parallel^2 \frac{\hat{\omega} - \hat{\omega}_{\star g}}{\hat{\omega} - \hat{k}_\parallel \hat{v}_\parallel - \hat{\omega}_D} \right\rangle$$
$$\times \delta\hat{A}_{\parallel m, n, \omega}(\mathbf{x}) \mathrm{e}^{i(m\theta + n\varphi - \omega t)}, \tag{B16}$$

with $\hat{}$ representing the normalized quantities. The parallel wave vector $k_\parallel$ is given by $k_\parallel = (m/q + n)/R_0$, and the magnetic drift frequency ω_D is given by $\omega_D = 2qn/r(m_e v_{\parallel,eq}^2 + \mu B_0)/(eZ_e B_0 R_0)$. Notice that $k_\parallel$ vanishes on the rational surface defined as $q = -m/n$. In the remainder of this paper, the eq subscript for the parallel velocity will be dropped for the sake of simplicity. Note that $\rho_\star$ gives the typical ordering between the equilibrium and the perturbed distribution function and $en_0 v_{th}$ is the normalization for the current. In this expression, we have introduced the generalized diamagnetic frequency $\omega_{\star g} = m T_{eq} \partial_{J_2} \log F_{eq}$, which includes all the spatial dependence of the equilibrium. For thermal passing particles, at lowest order in $\rho_\star$, one can write $J_2 \approx eZ_e \Phi$. Therefore, the derivative with respect to J_2 can be reduced to a derivative with respect to the radial position.

APPEND IX C: EQUILIBRIUM FREQUENCIES OF MOTION

The motion of a charged particle in toroidal geometry can be divided into a parallel and a drift motion (at lower order), $\mathbf{v} = v_\parallel \mathbf{b} + \mathbf{v}_g$, in which we omit the $\mathbf{E} \times \mathbf{B}$ drift. Note that this term can be added; however, one needs to be careful that it is independent of the toroidal motion so that the toroidal momentum can still be a motion invariant. The time evolution of the motion can be given by

$$\dot{\psi} = \mathbf{v} \cdot \nabla \psi, \tag{C1}$$

$$\dot{\theta} = v_\parallel \mathbf{b} \cdot \nabla \theta + \mathbf{v}_g \cdot \nabla \theta, \tag{C2}$$

$$\dot{\varphi} = v_\parallel q \mathbf{b} \cdot \nabla \theta + \mathbf{v}_g \cdot \nabla \varphi, \tag{C3}$$

where ψ is the poloidal flux and θ and φ are the poloidal and toroidal coordinates, respectively. The magnetic drift velocity $\mathbf{v}_g$ is given by

$$\mathbf{v}_g = \frac{m v_\parallel^2 + \mu B_0}{e B_0} \left(\mathbf{b}_0 \times \frac{\nabla B_0}{B_0} \right). \tag{C4}$$

The energy is defined as

$$E = \frac{1}{2} m v_\parallel^2 + \mu B(r, \theta) \tag{C5}$$

so that Eq. (C2) is expressed at lowest order in ρ_*, the Larmor radius normalized to the tokamak major radius, as follows:

$$\dot{\theta} = \epsilon_\parallel \sqrt{2/m} [E - \mu B_0(\theta)]^{1/2} \frac{\mathbf{B}_0 \cdot \nabla \theta}{B_0}. \tag{C6}$$

$\epsilon_\parallel$ designates the sign of the parallel velocity. We define the helical angle as $\zeta = \varphi - q\theta$. The time derivative of ζ gives

$$\dot{\zeta} = \dot{\varphi} - q(\bar{\psi})\dot{\theta}, \tag{C7}$$

where $\bar{\psi}$ is the flux surface at the resonance layer. Using Eq. (C2) and the fact that $q(\psi) - q(\bar{\psi}) = (\mathrm{d}q/\mathrm{d}r)\delta\psi$, we get

$$\dot{\zeta} = \frac{\mathrm{d}q}{\mathrm{d}\psi} \delta\psi \dot{\theta} + \mathbf{v}_g \cdot \nabla \zeta. \tag{C8}$$

It follows that the three angular motions are found to be the gyro-motion, the poloidal motion, and the toroidal motion (also called the bounce and precessional motions, for trapped particles). Their respective frequencies are written as

$$\Omega_1 = \Omega_b \oint \frac{\mathrm{d}\theta}{2\pi} \frac{1}{\dot{\theta}} \dot{\gamma} \approx \Omega_b \oint \frac{\mathrm{d}\theta}{2\pi} \frac{1}{\dot{\theta}} \frac{e B_0}{m}, \tag{C9}$$

$$\Omega_2 = \Omega_b \approx 2\pi \left(\oint \frac{\mathrm{d}\theta}{\dot{\theta}} \right)^{-1}, \tag{C10}$$

$$\Omega_3 = \Omega_b \oint \frac{\mathrm{d}\theta}{2\pi} \frac{1}{\dot{\theta}} \dot{\varphi} \approx \Omega_b \oint \frac{\mathrm{d}\theta}{2\pi} \frac{1}{\dot{\theta}} \mathbf{v}_g \cdot \left[-q'(\bar{\psi})\theta \nabla \psi \right. $$
$$\left. + \nabla \left((\varphi - q(\bar{\psi})\theta) \right) \right] + q(\bar{\psi}) \Omega_b \oint \frac{\mathrm{d}\theta}{2\pi}. \tag{C11}$$

Note that for passing particles, $\oint = \int_{-\pi}^{+\pi}$, whereas for trapped particles oscillating on $[-\theta_0, \theta_0]$, $\oint = \int_{-\theta_0}^{+\theta_0}$.

1. The poloidal frequency Ω_2

At the lowest order, the parallel velocity dominates the drift velocity, and the bounce frequency can be rewritten as

$$\Omega_2^{-1} = \oint \frac{\mathrm{d}\theta}{2\pi} \frac{1}{\mathbf{b} \cdot \nabla \theta} \frac{1}{v_\parallel}. \tag{C12}$$

We consider a simple circular equilibrium, with a large aspect ratio where the equilibrium magnetic field is given by

$$\mathbf{B}_0 = \nabla \psi \times \nabla \zeta. \tag{C13}$$

In this geometry, the magnitude of the equilibrium magnetic field can be expressed to the first order as $B_{(0)} = B_0(1 - \epsilon \cos \theta)$. Since $\mathbf{b} \cdot \nabla \theta \approx 1/qR$, we can write

$$\Omega_2^{-1} = \oint \frac{\mathrm{d}\theta}{2\pi} \frac{qR}{v_\parallel}. \tag{C14}$$

Taking into account that the major radius is expressed as

$$R = R_0(1 + \epsilon \cos \theta) \tag{C15}$$

and that the parallel velocity can be approximated in terms of the energy and radial position to the first order in ϵ as

$$v_\parallel = \epsilon_\parallel \sqrt{2(E - \mu B_{(0)})/m} = \epsilon_\parallel \sqrt{\frac{2E}{m}} \sqrt{1 - \frac{\mu B_{(0)}}{E}}, \tag{C16}$$

one can write Eq. (C14) as

$$\Omega_2^{-1} = \epsilon_\parallel q R_0 \sqrt{\frac{m}{2E}} \bar{\Omega}_b^{-1}, \tag{C17}$$

where $\epsilon_\parallel = sign(v_\parallel)$ and $\bar{\Omega}_b^{-1}$ is the integral given by

$$\bar{\Omega}_b^{-1} = \oint \frac{\mathrm{d}\theta}{2\pi} \frac{1}{\sqrt{1 - \lambda(1 - \epsilon \cos \theta)}}, \tag{C18}$$

with $\lambda = \mu B_0/E$. Keeping the first order effects in ϵ, we define a parameter κ which differentiates the magnetically trapping and passing particles

$$\kappa^2 = \frac{2\epsilon\lambda}{1 - (1 - \epsilon)\lambda}, \tag{C19}$$

and we rewrite Eq. (C18) as

$$\bar{\Omega}_b^{-1} = \frac{\kappa}{\sqrt{2\epsilon\lambda}} \oint \frac{\mathrm{d}\theta}{2\pi} \frac{1}{\sqrt{1 - \kappa^2 \sin^2(\theta/2)}}. \tag{C20}$$

The integral (C20) is to be solved separately for passing and trapped particles by integrating over the appropriate boundaries,

for passing particles, $(\kappa < 1): \theta_1 = -\pi, \theta_2 = +\pi,$ (C21)

for trapped particles, $(\kappa > 1): \theta_1 = -\theta_0, \theta_2 = +\theta_0.$ (C22)

Consequently, an appropriate change in variables is made for treating each class of particles. For passing particles, we make the change in variable $u = \theta/2$, and for trapped particles, $\sin u = \kappa \sin(\theta/2)$ such that $0 \le u \le \pi/2$ and $0 \le \theta \le \theta_0$. The integral (C20) is then expressed in terms of the elliptic integral of the first kind $\mathbb{K}(m)$ as defined in Ref. 34,

$$\mathbb{K}(m) = \int_0^{\pi/2} d\theta \frac{1}{\sqrt{1 - m \sin^2\theta}}. \tag{C23}$$

It finally comes that

$$\bar{\Omega}_b^{-1} = \frac{\kappa}{\sqrt{2\epsilon\lambda}} \frac{2}{\pi} \begin{cases} \mathbb{K}(\kappa^2) & \text{for passing particles} \\ \frac{1}{\kappa} \mathbb{K}(1/\kappa^2) & \text{for trapped particles.} \end{cases} \tag{C24}$$

Finally, the poloidal frequency Ω_2 is calculated for passing and trapped particles, locally, in circular geometry to the leading order in ϵ, and it is expressed as

$$\Omega_2 = \epsilon_\parallel \frac{q}{R_0} \sqrt{\frac{2E}{m}} \frac{\sqrt{2\epsilon\lambda}}{\kappa} \frac{\pi}{2} \begin{cases} \mathbb{K}^{-1}(\kappa^2), & \kappa < 1 \\ \kappa\,\mathbb{K}^{-1}(1/\kappa^2), & \kappa > 1. \end{cases} \tag{C25}$$

2. The toroidal frequency Ω_3

The precessional frequency is given to the first order in ϵ by

$$\Omega_3 = \bar{\Omega}_b \oint \frac{d\theta}{2\pi} \frac{\mu B_{(0)} + m v_\parallel^2}{\sqrt{1 - \lambda(1 - \epsilon\cos\theta)}} \frac{\mathbf{B}_{(0)} \times \nabla B_{(0)}}{e B_{(0)}^3}$$
$$\cdot \left[-\frac{dq}{d\psi} s\theta\nabla\psi + \nabla\zeta \right] + q(\bar{\psi})\Omega_b \oint \frac{d\theta}{2\pi}. \tag{C26}$$

In order to evaluate the integral in Eq. (C26), we explicit the projection of the curvature term onto $\nabla\psi$ and $\nabla\zeta$ using Eq. (C13),

$$(\mathbf{B}_0 \times \nabla B_0).\nabla\psi = -\nabla B_0 \cdot (\nabla\psi \times \nabla B_0)$$
$$= -\nabla B_0 \cdot [\nabla\psi \times (\nabla\psi \times \nabla\zeta)]$$
$$= -|\nabla\psi|^2 |\nabla\zeta|^2 (\partial B_0/\partial\zeta), \tag{C27}$$

$$(\mathbf{B}_0 \times \nabla B_0).\nabla\zeta = \nabla B_0 \cdot (\nabla\zeta \times \nabla B_0)$$
$$= -\nabla B_0 \cdot [\nabla\zeta \times (\nabla\psi \times \nabla\zeta)]$$
$$= -|\nabla\zeta|^2 |\nabla\psi|^2 (\partial B_0/\partial\psi). \tag{C28}$$

Writing $\mu B_0 + m v_\parallel^2 = 2E - \mu B_0$, the expression of the toroidal frequency Ω_3 becomes

$$\Omega_3 = \bar{\Omega}_b \frac{E B_0}{e R_0 B_0^3} |\nabla\zeta|^2 |\nabla\Psi| \oint \frac{d\theta}{2\pi} \frac{(2 - \lambda)(s\theta\sin\theta + \cos\theta)}{\sqrt{1 - \lambda(1 - \epsilon\cos\theta)}}$$
$$+ \delta_{passing} q(r)\Omega_2. \tag{C29}$$

Since $d\psi/dr = B_0 r/q$ and $|\nabla\zeta| \approx q/r$, it follows that Eq. (C29) is written as

$$\Omega_3 = \frac{q}{r} \frac{E}{e B_0 R_0} \bar{\Omega}_d + \delta_{passing} q(r)\Omega_2, \tag{C30}$$

where $\bar{\Omega}_d$ is given in terms of Ω_2 given by Eq. (C25),

$$\bar{\Omega}_d = \bar{\Omega}_b (2 - \lambda)\Omega_\kappa. \tag{C31}$$

With $2 - \lambda = \frac{4\epsilon + \kappa^2(1 - 2\epsilon)}{2\epsilon + (1 - \epsilon)\kappa^2}$, and Ω_κ, which is the integral, is given by

$$\Omega_\kappa = \int_{\theta_1}^{\theta_2} \frac{d\theta}{2\pi} \frac{(s\theta\sin\theta + \cos\theta)}{\sqrt{1 - \lambda(1 - \epsilon\cos\theta)}}. \tag{C32}$$

The integral (C32) is also solved separately for passing and trapped particles by integrating over the appropriate boundaries given in Eqs. (C21) and (C22). For the $\cos\theta$ integral, we notice that $\cos\theta = 1 - \sin^2\frac{\theta}{2}$, and so the convenient change in variable would be $u = \theta/2$ for passing particles and $\sin u = \sin\theta/2$ for trapped particles. As for the $\sin\theta$ integral, we solve it integrating by parts as we notice that

$$\frac{d}{d\theta}\left(\sqrt{1 - \kappa^2\sin^2\frac{\theta}{2}}\right) = -\frac{\kappa^2}{2} \frac{\sin\theta}{2\sqrt{1 - \kappa^2\sin^2\frac{\theta}{2}}}. \tag{C33}$$

Therefore,

$$\int_{\theta_1}^{\theta_2} \frac{d\theta}{2\pi} \frac{\theta\sin\theta}{\sqrt{1 - \kappa^2\sin^2\frac{\theta}{2}}} = -\frac{4}{\kappa^2}\left[\frac{\theta}{2\pi}\sqrt{1 - \kappa^2\sin^2\left(\frac{\theta}{2}\right)}\right]_{\theta_1}^{\theta_2}$$
$$+ \frac{4}{\kappa^2}\int_{\theta_1}^{\theta_2} \frac{d\theta}{2\pi}\sqrt{1 - \kappa^2\sin^2\left(\frac{\theta}{2}\right)}. \tag{C34}$$

The term between brackets is equal to zero for trapped particles, as $\kappa^2\sin^2(\theta/2) = 1$ for $\theta = \pm\theta_0$. However, for passing particles, $\theta_1 = -\pi$ and $\theta_2 = +\pi$, it does not vanish and it gives $\sqrt{1 - \kappa^2}$. Using the standard definition of the complete elliptic integrals of the first kind given by (C23) and that of the second kind given by[34]

$$\mathbb{E}(m) = \int_0^{\pi/2} d\theta\sqrt{1 - m\sin^2\theta}, \tag{C35}$$

the frequency $\bar{\Omega}_d$ can be expressed as

$$\bar{\Omega}_d = \begin{cases} \dfrac{4\epsilon + \kappa^2(1 - 2\epsilon)}{2\epsilon + (1 - \epsilon)\kappa^2}\left[1 + \dfrac{2}{\kappa^2}\left(\dfrac{\mathbb{E}(\kappa^2)}{\mathbb{K}(\kappa^2)} - 1\right) + \dfrac{4s}{\kappa^2}\left(\dfrac{\mathbb{E}(\kappa^2)}{\mathbb{K}(\kappa^2)} - \dfrac{\pi}{2}\dfrac{\sqrt{1 - \kappa^2}}{\mathbb{K}(\kappa^2)}\right)\right] & \text{for passing particles}(\kappa < 1) \\[4ex] \dfrac{4\epsilon + \kappa^2(1 - 2\epsilon)}{2\epsilon + (1 - \epsilon)\kappa^2}\left[2\dfrac{\mathbb{K}(1/\kappa^2)}{\mathbb{E}(1/\kappa^2)} - 1 + 4s\left(\dfrac{\mathbb{K}(1/\kappa^2)}{\mathbb{E}(1/\kappa^2)} + \dfrac{1}{\kappa^2} - 1\right)\right] & \text{for trapped particles}(\kappa > 1). \end{cases} \tag{C36}$$

APPENDIX D: IMPACT OF THE MAGNETIC FIELD CURVATURE ON THE TEARING INSTABILITY THROUGH MODE-MODE COUPLING

In Secs. II–IV, we have considered a single harmonic for the perturbation, thus neglecting possible couplings between the different harmonics. However, multiple rational surfaces may be present within the domain and so allow double tearing modes and toroidal coupling of modes, a process which is known to be stabilizing.[6] We have also neglected the electrostatic potential and treated the instability in a purely magnetic approach. Of course, although they can be insightful, these approximations make our model less accurate as we neglect some physical mechanisms that are important in understanding the role of the magnetic curvature. For this reason, we investigate in this section the effect of the curvature through toroidal coupling of main resonating mode, which we consider here as the principal harmonic and one of its side bands. The electrostatic potential is considered here. However, the Poisson equation is not solved because we use the ideal MHD condition outside of the resonant surface to relate ϕ to $A_\parallel$. We start with the electromagnetic drift kinetic equation that describes the electron dynamics. The perturbed distribution function δF is decomposed into adiabatic and nonadiabatic parts,

$$\delta F = \frac{e}{T_{eq}} F_{eq}\phi + g, \tag{D1}$$

where F_{eq} is the background distribution, considered as a Maxwellian, and g is the nonadiabatic distribution function, satisfying the equation

$$(\omega - k_\parallel v_\parallel - \omega_D)g = -(\omega - \omega_\star)\frac{eF_{eq}}{T_{eq}}(\phi - v_\parallel A_\parallel), \tag{D2}$$

where ϕ and $A_\parallel$ are the perturbed electrostatic potential and the parallel component of the magnetic vector potential, respectively. In this equation, the magnetic drift frequency is expressed as a differential operator,

$$\omega_D = -i\mathbf{v}_D \cdot \nabla = \frac{v_\parallel^2 + \mu B}{eB_0 R_0}\left(\sin\theta\frac{\partial}{\partial r} + \cos\theta\frac{\partial}{r\partial\theta}\right), \tag{D3}$$

r and θ are the radial coordinate and the poloidal angle, respectively. We consider the toroidal coupling of modes m and $m+1$, where m is the poloidal wave number. Perturbations are then expressed in the form

$$Q = Q_m e^{im\theta} + Q_{m+1} e^{i(m+1)\theta}. \tag{D4}$$

Assuming $\partial_r g_m = \partial_r g_{m+1} = 0$ and separating the main oscillating component from the sideband, the Vlasov equation is rewritten as

$$\mathcal{M}\begin{pmatrix} g_m \\ g_{m+1} \end{pmatrix} = S\begin{pmatrix} \phi_m - v_\parallel A_{\parallel m} \\ \phi_{m+1} - v_\parallel A_{\parallel m+1} \end{pmatrix}, \tag{D5}$$

where the matrix $\mathcal{M}$ is the square matrix,

$$\mathcal{M} = \begin{pmatrix} \omega - k_{\parallel m}v_\parallel & \dfrac{i(m+1)}{2r}v_D \\ \dfrac{im}{2r}v_D & \omega - k_{\parallel m+1}v_\parallel \end{pmatrix}, \tag{D6}$$

$S = -(\omega - \omega_{\star n})eF_{eq}/T_{eq}$, $v_D = (v_\parallel^2 + \mu B)/eB_0 R_0$, and B_0 is the equilibrium magnetic field. The parallel wave vector $k_\parallel$ takes a different form depending on the considered poloidal mode such that $k_{\parallel m} = (m/q_m + n)/R$ is evaluated at the resonant surface r_m and $k_{\parallel m+1} = ((m+1)/q_{m+1} + n)/R$ at the resonant surface r_{m+1}. The solution of Eq. (D5) can be obtained by inverting the matrix $\mathcal{M}$,

$$\mathcal{M}^{-1} = \frac{1}{|\mathcal{M}|}\begin{pmatrix} \omega - k_{\parallel m+1}v_\parallel & -\dfrac{i(m+1)}{2r}v_D \\ -\dfrac{im}{2r}v_D & \omega - k_{\parallel m}v_\parallel \end{pmatrix}, \tag{D7}$$

where $|\mathcal{M}| = \det(\mathcal{M}) = (\omega - k_{\parallel m}v_\parallel)(\omega - k_{\parallel m+1}v_\parallel) + v_D^2 m(m+1)/4r^2$ is the determinant of matrix $\mathcal{M}$. The dispersion relation of the tearing mode is obtained by integrating Ampère's law for each mode. In the constant-ψ approximation, this reads in normalized units

$$\delta_e^2 \Delta_m' A_{\parallel m} = 2\pi \int_{\mathbb{R}} dx \int dv_\parallel v_\perp dv_\perp v_\parallel g_m, \tag{D8}$$

$$\delta_e^2 \Delta_{m+1}' A_{\parallel m+1} = 2\pi \int_{\mathbb{R}} dx \int dv_\parallel v_\perp dv_\perp v_\parallel g_{m+1}. \tag{D9}$$

In the matrix form, this system of equations can be written as

$$\begin{pmatrix} \Delta_m' & 0 \\ 0 & \Delta_{m+1}' \end{pmatrix}\begin{pmatrix} A_{\parallel m} \\ A_{\parallel m+1} \end{pmatrix} = \mathcal{I}\begin{pmatrix} A_{\parallel m} \\ A_{\parallel m+1} \end{pmatrix}, \tag{D10}$$

where $\mathcal{I}$ is a matrix that will be calculated in the following. The perturbed distribution functions associated with modes m and $m+1$ at the resonant surfaces r_m and r_{m+1} are expressed, respectively, in normalized units as

$$g_m = -\frac{(\omega - k_{\parallel m+1}v_\parallel)(\phi_m - 2v_\parallel A_{\parallel m}) - i\dfrac{m+1}{2r}v_D(\phi_{m+1} - 2v_\parallel A_{\parallel m+1})}{(\omega - k_{\parallel m}v_\parallel)(\omega - k_{\parallel m+1}v_\parallel) + \dfrac{m(m+1)}{4r^2}v_D^2}$$
$$\times (\omega - \omega_{\star n})\frac{1}{T_{eq}}\frac{n_e}{(\pi T_{eq})^{3/2}}e^{-\frac{v_\parallel^2 + v_\perp^2}{T_{eq}}}, \tag{D11}$$

$$g_{m+1} = -\frac{-i\dfrac{m}{2r}v_D(\phi_m - 2v_\parallel A_{\parallel m}) + (\omega - k_{\parallel m}v_\parallel)(\phi_{m+1} - 2v_\parallel A_{\parallel m+1})}{(\omega - k_{\parallel m}v_\parallel)(\omega - k_{\parallel m+1}v_\parallel) + \dfrac{m(m+1)}{4r^2}v_D^2}$$
$$\times (\omega - \omega_{\star n})\frac{1}{T_{eq}}\frac{n_e}{(\pi T_{eq})^{3/2}}e^{-\frac{v_\parallel^2 + v_\perp^2}{T_{eq}}}. \tag{D12}$$

Therefore, the response of mode m is given by the combination of the modes m and $m+1$ of the potential. The same can be said about the mode $m+1$. The integrals in Eqs. (D8) (first line of matrix $\mathcal{I}$) and (D9) (second line of matrix $\mathcal{I}$) are calculated around the resonant surfaces r_m and r_{m+1}, respectively.

The resonant condition $\omega - k_\parallel v_\parallel$ at one of the resonant surfaces can be simplified when evaluated at the other surface. In fact, away from the resonant surface r_m, the parallel streaming motion is much faster than the frequency of the mode; however, close to that surface, the resonance is satisfied and one can write $\omega - k_{\parallel m}v_\parallel \approx 0$. This allows us to write

$$(\omega - k_{\parallel m+1} v_\parallel)|_{r_m} = \omega - \left(\frac{m+1}{q_{m+1}} + n \right)\Bigg|_{r_m} v_\parallel$$

$$= \omega - k_{\parallel m} v_\parallel - \frac{v_\parallel}{q_{m+1}} \approx -\frac{v_\parallel}{q_{m+1}}, \qquad (D13)$$

$$(\omega - k_{\parallel m} v_\parallel)|_{r_{m+1}} = \omega - \left(\frac{m}{q_m} + n \right)\Bigg|_{r_{m+1}} v_\parallel$$

$$= \omega - k_{\parallel m+1} v_\parallel - \frac{v_\parallel}{q_m} \approx \frac{v_\parallel}{q_m} \qquad (D14)$$

in normalized units. Therefore, we have implicitly normalized the frequencies to the transit frequency $\omega_t = v_{\text{th}}/R_0$.

We assume that the magnetic drift is constant on each of the resonant surfaces (the local approximation). Inside the resonant layer, we consider that the corresponding electrostatic potential is equal to zero. Outside of it, the ideal MHD condition applies, i.e., the parallel electric field vanishes at that position. Therefore, on the resonance surface r_m, $E_{\parallel m+1} = 0$, i.e., $\phi_{m+1} = 2\omega A_{\parallel m+1} k_{\parallel m+1}^{-1}$, and on $r_m + 1$, $E_{\parallel m} = 0$, i.e., $\phi_m = 2\omega A_{\parallel m} k_{\parallel m}^{-1}$. On these grounds, we calculate each term of matrix $\mathcal{I}$ of Eq. (D10),

$$\mathcal{I}_{m,m} \approx -\frac{1}{\delta_e^2} \frac{4\pi}{T_{\text{eq}}} \int dv_\parallel v_\perp dv_\perp \frac{v_\parallel^3}{q_{m+1}} (\omega - \omega_\star) \frac{n_e}{(\pi T_{\text{eq}})^{3/2}} e^{-\frac{v_\parallel^2 + v_\perp^2}{T_{\text{eq}}}} \frac{q_{m+1}}{v_\parallel}$$

$$\times \int dx \frac{1}{k_{\parallel m}' x v_\parallel - \omega + \frac{m(m+1)v_D^2 q_{m+1}}{4 r_m^2 v_\parallel}}, \qquad (D15)$$

$$\mathcal{I}_{m,m+1} = -i \frac{1}{\delta_e^2} \frac{4\pi}{T_{\text{eq}}} \int dv_\parallel v_\perp dv_\perp (\omega - \omega_\star) \frac{n_e}{(\pi T_{\text{eq}})^{3/2}}$$

$$\times e^{-\frac{v_\parallel^2 + v_\perp^2}{T_{\text{eq}}}} q_{m+1} \frac{m+1}{2r_m} v_D$$

$$\times \Bigg\{ \int dx \frac{\omega}{k_{\parallel m+1}' k_{\parallel m}' v_\parallel x^2 - \omega k_{\parallel m+1}' x + \frac{m(m+1)v_D^2 q_{m+1}}{4 r_m^2 v_\parallel} k_{\parallel m+1}' x}$$

$$+ v_\parallel \int dx \frac{1}{k_{\parallel m}' x v_\parallel - \omega + \frac{m(m+1)v_D^2 q_{m+1}}{4 r_m^2}} \Bigg\} \qquad (D16)$$

After integration over x and $v_\perp$ and using the definition of the complex logarithm, the matrix elements $\mathcal{I}_{m,m}$ and $\mathcal{I}_{m,m+1}$ become $\mathcal{I}_{m,m} = -i \frac{1}{\delta_e^2} \frac{4\sqrt{\pi} n_{\text{eq}}}{|k_{\parallel m}'| \sqrt{T_{\text{eq}}}} [\omega - \omega_{\star n}(1 + (2T_{\text{eq}} - \frac{3}{2})\eta_e)]$ and $\mathcal{I}_{m,m+1} = 0$.

Similar calculations for $\mathcal{I}_{m+1,m}$ and $\mathcal{I}_{m+1,m+1}$ lead to the matrix $\mathcal{I}$,

$$\mathcal{I} = -i \frac{1}{\delta_e^2} \frac{4\sqrt{\pi} n_{\text{eq}}}{\sqrt{T_{\text{eq}}}} \left[\omega - \omega_{\star n} \left(1 + \left(2T_{\text{eq}} - \frac{3}{2} \right) \eta_e \right) \right]$$

$$\times \begin{pmatrix} \dfrac{1}{|k_{\parallel m}'|} & 0 \\ 0 & \dfrac{1}{|k_{\parallel m+1}'|} \end{pmatrix}, \qquad (D17)$$

with vanishing nondiagonal terms. Looking for nontrivial solutions of Eq. (D10) is equivalent to solving the equation,

$$\left(\Delta_m' + \frac{\Gamma}{|k_{\parallel m}'|} \right) \left(\Delta_{m+1}' + \frac{\Gamma}{|k_{\parallel m+1}'|} \right) = 0, \qquad (D18)$$

where Γ reads

$$\Gamma = i \frac{1}{\delta_e^2} \frac{4\sqrt{\pi} n_{\text{eq}}}{\sqrt{T_{\text{eq}}}} \left[\omega - \omega_{\star n} \left(1 + \left(2T_{\text{eq}} - \frac{3}{2} \right) \eta_e \right) \right]. \qquad (D19)$$

The solutions for the modes m and $m + 1$ are therefore decoupled from each other. This indicates that there is no effect of the curvature of the field on the stability of the tearing mode in the absence of particle trapping.

APPENDIX E: MAGNETIC HAMILTONIAN FOR DEEPLY TRAPPED PARTICLES

Without any loss of generality, the Hamiltonian can be decomposed into equilibrium and perturbed components, namely,

$$\mathcal{H} = \mathcal{H}_{eq} + \delta \mathcal{H}_{A_\parallel}, \qquad (E1)$$

where the equilibrium Hamiltonian is simply

$$\mathcal{H}_{eq} = \frac{1}{2} m v_\parallel^2 + \mu B \qquad (E2)$$

and the perturbed Hamiltonian is, for the case of electrons,

$$\delta \mathcal{H}_{A_\parallel} = e v_\parallel A_\parallel. \qquad (E3)$$

The parallel component of the perturbed vector potential is written as a single helicity perturbation in real space,

$$A_\parallel = A_\parallel e^{i(m\theta + n\varphi)}, \qquad (E4)$$

where $A_\parallel$ is the amplitude of the perturbation and the time dependence has been omitted for the sake of clarity. However, the perturbations introduced here exist in real space and do not have the same expression in the space of canonically conjugated variables that are suitable for the description of particle trajectories. Therefore, the Hamiltonian needs to be written in terms of the action-angle variables of the deeply trapped particles. For this purpose, we use the relations

$$\theta = \theta_0 \sin \alpha_2, \qquad (E5)$$

$$\varphi = \alpha_3 + q\theta_0 \sin \alpha_2, \qquad (E6)$$

where θ_0 is the bounce poloidal angle. Note that the previous expressions, although strictly speaking valid for deeply trapped particles, can be applied for poloidal angles up to $\theta_0 \approx \pi/2$ and therefore also for trapped particles (not barely trapped particles though). Moreover, the parallel velocity can be expressed in terms of the angle α_2,

$$v_\parallel = v_{\parallel 0} \cos \alpha_2, \qquad (E7)$$

where $v_{\parallel 0}$ is the parallel velocity on the midplane.

Introducing the expressions E5 and E6 that provide θ and φ as functions of α_2 and α_3, the parallel component of the vector potential is then expressed as

$$A_\parallel = A_\parallel e^{i(m+nq)\theta_0 \sin \alpha_2} e^{in\alpha_3}. \qquad (E8)$$

Using the Jacobi-Anger expansion,

$$e^{ix\cos\alpha} = \sum_{p=-\infty}^{\infty} i^p J_p(x) e^{ip\alpha}, \tag{E9}$$

where $J_p(x)$ is the Bessel function of the first kind of order p, we can write the perturbed Hamiltonian as

$$\delta\mathcal{H}_{A_\parallel} = ev_{\parallel 0}A_\parallel \frac{1}{2}e^{in\alpha_3}\left(e^{i\alpha_2}+e^{-i\alpha_2}\right)\sum_{p=-\infty}^{\infty} J_p\big((m+nq)\theta_0\big)e^{ip\alpha_2}. \tag{E10}$$

The multiplication by $v_\parallel$ introduces therefore a shift in the p summation index,

$$\delta\mathcal{H}_{A_\parallel} = ev_{\parallel 0}A_\parallel \sum_{n_2=-\infty}^{\infty} \frac{n_2 J_{n_2}\big((m+nq)\theta_0\big)}{(m+nq)\theta_0}e^{in_2\alpha_2}e^{in\alpha_3}, \tag{E11}$$

where we have used the property

$$J_{p+1}(x) + J_{p-1}(x) = \frac{2p}{x}J_p(x). \tag{E12}$$

Finally, the n_2, n_3, ω components of the perturbed Hamiltonian are found to be

$$\delta\mathcal{H}_{A_\parallel,n_2,n_3,\omega} = ev_{\parallel 0}A_\parallel \frac{n_2 J_{n_2}\big((m+nq)\theta_0\big)}{(m+nq)\theta_0}, \tag{E13}$$

which reduces to $\delta\mathcal{H}_{A_\parallel,n_2=0,n_3,\omega} = 0$.

REFERENCES

[1] X. G. Wang, A. Bhattacharjee, and A. T. Y. Lui, "Collisionless tearing instability in magnetotail plasmas," J. Geophys. Res.-Space Phys. **95**(A9), 15047–15057, https://doi.org/10.1029/JA095iA09p15047 (1990).

[2] E. M. Carolipio, W. W. Heidbrink, C. B. Forest, and R. B. White, "Simulations of beam ion transport during tearing modes in the DIII-D tokamak," Nucl. Fusion **42**(7), 853 (2002).

[3] M. García-Muñoz, P. Martin, H.-U. Fahrbach, M. Gobbin, S. Günter, M. Maraschek, L. Marrelli, H. Zohm et al., "NTM induced fast ion losses in ASDEX-Upgrade," Nucl. Fusion **47**(7), L10 (2007).

[4] O. Sauter, C. Angioni, and Y. R. Lin-Liu, "Neoclassical conductivity and bootstrap current formulas for general axisymmetric equilibria and arbitrary collisionality regime," Phys. Plasmas **6**(7), 2834–2839 (1999).

[5] H. P. Furth, J. Killeen, and M. N. Rosenbluth, "Finite-resistivity instabilities of a sheet pinch," Phys. Fluids **6**(4), 459–484 (1963).

[6] A. H. Glasser, J. M. Greene, and J. L. Johnson, "Resistive instabilities in general toroidal plasma configurations," Phys. Fluids **18**(7), 875–888 (1975).

[7] J. F. Drake and Y. C. Lee, "Nonlinear evolution of collisionless and semicollisional tearing modes," Phys. Rev. Lett. **39**(8), 453–456 (1977).

[8] J. F. Drake and Y. C. Lee, "Kinetic theory of tearing instabilities," Phys. Fluids **20**(8), 1341–1353 (1977).

[9] Y. Q. Liu, R. J. Hastie, and T. C. Hender, "Modification of Δ' by magnetic feedback and kinetic effects," Phys. Plasmas **19**(9), 092510 (2012).

[10] R. D. Hazeltine, D. Dobrott, and T. S. Wang, "Kinetic theory of tearing instability," Phys. Fluids **18**(12), 1778–1786 (1975).

[11] J. W. Connor, S. C. Cowley, and R. J. Hastie, "Micro-tearing stability in tokamaks," Plasma Phys. Controlled Fusion **32**(10), 799–817 (1990).

[12] A. Zocco, N. F. Loureiro, D. Dickinson, R. Numata, and C. M. Roach, "Kinetic microtearing modes and reconnecting modes in strongly magnetised slab plasmas," Plasma Phys. Controlled Fusion **57**(6), 065008 (2015).

[13] R. Fitzpatrick and F. Porcelli, "Collisionless magnetic reconnection with arbitrary guide field," Phys. Plasmas **11**(10), 4713–4718 (2004).

[14] F. Porcelli, "Collisionless m = 1 tearing mode," Phys. Rev. Lett. **66**(4), 425 (1991).

[15] H. Lutjens, J. F. Luciani, and X. Garbet, "Curvature effects on the dynamics of tearing modes in tokamaks," Phys. Plasmas **8**(10), 4267–4270 (2001).

[16] D. J. Liu, J. Bao, T. Han, J. Q. Wang, and Z. H. Lin, "Verification of gyrokinetic particle simulation of current-driven instability in fusion plasmas. III. Collisionless tearing mode," Phys. Plasmas **23**(2), 022502 (2016).

[17] W. Wan, Y. Chen, and S. E. Parker, "Gyrokinetic δf simulation of the collisionless and semicollisional tearing mode instability," Phys. Plasmas **12**(1), 012311 (2005).

[18] R. D. Sydora, "Nonlinear dynamics of small-scale magnetic islands in high temperature plasmas," Phys. Plasmas **8**(5), 1929–1934 (2001).

[19] Y. Chen, J. Chowdhury, N. Maksimovic, S. E. Parker, and W. Wan, "Gyrokinetic-ion drift-kinetic-electron simulation of the (m = 2, n = 1) cylindrical tearing mode," Phys. Plasmas **23**(5), 056101 (2016).

[20] R. Hatzky, A. Käunies, and A. Mishchenko, "Electromagnetic gyrokinetic PIC simulation with an adjustable control variates method," J. Comput. Phys. **225**(1), 568–590 (2007).

[21] W. A. Hornsby, P. Migliano, R. Buchholz, L. Kroenert, A. Weikl, A. G. Peeters, D. Zarzoso, E. Poli, and F. J. Casson, "The linear tearing instability in three dimensional, toroidal gyro-kinetic simulations," Phys. Plasmas **22**(2), 022118 (2015).

[22] W. A. Hornsby, P. Migliano, R. Buchholz, S. Grosshauser, A. Weikl, D. Zarzoso, F. J. Casson, E. Poli, and A. G. Peeters, "The non-linear evolution of the tearing mode in electromagnetic turbulence using gyrokinetic simulations," Plasma Phys. Controlled Fusion **58**(1), 014028 (2016).

[23] O. Zacharias, R. Kleiber, and R. Hatzky, "Gyrokinetic simulations of collisionless tearing modes," J. Phys. Conf. Ser. **401**, 012026 (2012).

[24] P. J. Catto and M. N. Rosenbluth, "Trapped electron modifications to tearing modes in the low collision frequency limit," Phys. Fluids **24**(2), 243–255 (1981).

[25] A. K. Swamy, R. Ganesh, S. Brunner, J. Vaclavik, and L. Villard, "Collisionless microtearing modes in hot tokamaks: Effect of trapped electrons," Phys. Plasmas **22**(7), 072512 (2015).

[26] D. Dickinson, C. M. Roach, S. Saarelma, R. Scannell, A. Kirk, and H. R. Wilson, "Microtearing modes at the top of the pedestal," Plasma Phys. Controlled Fusion **55**(7), 074006 (2013).

[27] J. Chowdhury, Y. Chen, W. G. Wan, S. E. Parker, W. Guttenfelder, and J. M. Canik, "Particle-in-cell δf gyrokinetic simulations of the microtearing mode," Phys. Plasmas **23**(1), 012513 (2016).

[28] S. Moradi, I. Pusztai, W. Guttenfelder, T. Fulop, and A. Mollen, "Microtearing modes in spherical and conventional tokamaks," Nucl. Fusion **53**(6), 063025 (2013).

[29] A. K. Swamy, R. Ganesh, J. Chowdhury, S. Brunner, J. Vaclavik, and L. Villard, "Global gyrokinetic stability of collisionless microtearing modes in large aspect ratio tokamaks," Phys. Plasmas **21**(8), 082513 (2014).

[30] D. Edery, X. Garbet, J.-P. Roubin, and A. Samain, "Variational formalism for kinetic-MHD instabilities in tokamaks," Plasma Phys. Controlled Fusion **34**(6), 1089 (1992).

[31] A. Mishchenko, R. Hatzky, and A. Könies, "Conventional δf-particle simulations of electromagnetic perturbations with finite elements," Phys. Plasmas **11**(12), 5480–5486 (2004).

[32] J. Daintith and E. Wright, A Dictionary of Computing (OUP, Oxford, 2008).

[33] J. Wesson, Tokamaks (Oxford University Press, 2011), Vol. 149.

[34] M. Abramowitz, I. A. Stegun et al., Handbook of Mathematical Functions with Formulas, Graphs, and Mathematical Tables (Dover, New York, 1972), Vol. 9.

[35] A. G. Peeters, Y. Camenen, F. James Casson, W. A. Hornsby, A. P. Snodin, D. Strintzi, and G. Szepesi, "The nonlinear gyro-kinetic flux tube code GKW," Comput. Phys. Commun. **180**(12), 2650–2672 (2009).

[36] A. K. Sundaram and A. Sen, "Gyrokinetic analysis of tearing instabilities in a collisionless plasma," Phys. Plasmas **18**(3), 032112 (2011).

[37] S. Nasr, A. I. Smolyakov, P. Migliano, D. Zarzoso, X. Garbet, and S. Benkadda, "Interchange destabilization of collisionless tearing modes by temperature gradient," Phys. Plasmas **25**(7), 074503 (2018).

[38] M. Hoshino, "The electrostatic effect for the collisionless tearing mode," J. Geophys. Res.: Space Phys. **92**(A7), 7368–7380, https://doi.org/10.1029/JA092iA07p07368 (1987).